JACS
JOURNAL OF THE AMERICAN CHEMICAL SOCIETY
Article
pubs.acs.org/JACS

Lyotropic Chiral Nematic Liquid Crystalline Aliphatic Conjugated Polymers Based on Disubstituted Polyacetylene Derivatives That Exhibit High Dissymmetry Factors in Circularly Polarized Luminescence

Benedict A. San Jose, Satoshi Matsushita, and Kazuo Akagi*

Department of Polymer Chemistry, Kyoto University, Katsura, Kyoto 615-8510, Japan

Supporting Information

ABSTRACT: We synthesized disubstituted liquid crystalline polyacetylene (diLCPA) derivatives bearing 4-nonyloxy phenyl groups with lyotropic and thermotropic LC behavior. The poly(diphenylacetylene) main chain structure of the diLCPAs and the chirality induced with either chiral moieties or chiral dopants allow the formation of a highly ordered lyotropic N*-LC phase. Circular dichroism (CD) spectra of the diLCPAs imply that one-handed intrachain helical structures are formed in solution, while interchain helical π-stacking between the polymer main chains are formed in cast film and in the N*-LC state. Absorption dissymmetry factors (g_{abs}) in the N*-LC state show values on the order of 10^{-1}. The N*-LC state facilitates the formation of helically π-stacked structures with a high degree of helical ordering of the diLCPA and is indispensable for the generation of circularly polarized luminescence (CPL) with high emission dissymmetry factors (g_{em}) on the order of 10^{-1}. To the best of our knowledge, this is the highest reported value of CPL achieved for aliphatic, conjugated polymers. As an alternative to the thermotropic N*-LC phase, we have found that the lyotropic N*-LC phase of diLCPA could be promising materials possessing CPL functionality for use in next-generation π-conjugated organic optoelectronic devices, displays, and sensors.

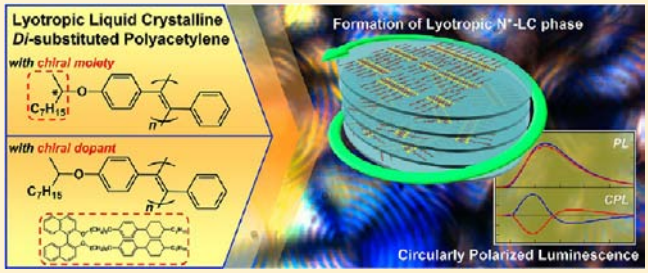

1. INTRODUCTION

Circularly polarized luminescence (CPL) of organic and polymeric materials has attracted considerable interest in photonic devices, such as light-emitting diodes, optical amplifiers, and optical information storage.[1,2] CPL can also be used to illuminate liquid crystal displays (LCDs). As a specific example, LCDs using a CPL backlight have been shown to exhibit several advantages, including steeper transmission-voltage characteristics and higher brightness, compared with LCDs using linearly polarized luminescence (LPL) illumination.[1] Hence, considerable effort has been devoted to the generation of CPL emission using various materials and methods.

CPL from conjugated polymer systems was first reported using polythiophene (PT) having a chiral side chain with emission dissymmetry factors (g_{em}) values of up to 5.0×10^{-3}.[3] Subsequently, circularly polarized electroluminescence (CPEL)[2] was reported using an EL cell with poly(*p*-phenylenevinylene) (PPV) bearing a chiral side chain as an emissive layer. The CPEL device has reported values of g_{em} up to -1.7×10^{-3}. In chiral substituted conjugated polymers, the chiroptical properties are assumed to evolve mainly from interchain interactions within chiral aggregates. There has been a CPEL device described that is constructed with a thermotropic liquid crystalline polyfluorene (PF) bearing chiral side chains with g_{em} values of up to -2.5×10^{-1}.[4] The combination of well-defined chiral packing of the liquid crystalline PF as well as chiral interchain interactions is the key for the increase in g_{em} values of the PF-based CPEL device. Subsequently, CPL in other aromatic conjugated polymers has also been reported.[5,6]

Meanwhile, research concerning the generation of CPL from chiral nematic liquid crystal (N*-LC) materials has been pursued. Liquid crystals (LCs) are anisotropic fluids of supramolecular assemblies that exist as an intermediate phase between isotropic fluid and solid crystal phases. LCs can be classified as either thermotropic or lyotropic.[7] N*-LC materials exhibit optical activity, circular dichroism (CD), and even selective reflection at specific wavelengths of circularly polarized light of a certain handedness.[8]

The first approach to produce CPL with high g_{em} involved using a fluorescent dye embedded in a N*-LC host.[9] Recently, this research was expanded to include CPL generated within the selective reflection band of the N*-LC[10] and wavelength-tunable CPL.[8] Furthermore, N*-LCs are used as platforms for the generation of low-threshold lasing,[11,12] and CPL lasers.[12] These developments demonstrate that the supramolecular helical ordering of the N*-LC phase can be utilized to generate CPL with high g_{em} values.

Received: August 31, 2012
Published: November 14, 2012

dx.doi.org/10.1021/ja3086565 | J. Am. Chem. Soc. 2012, 134, 19795−19807

One-handed helical conjugated polymers can be excellent N*-LC materials for the generation of CPL, due to their fluorescence and their ability to exhibit LC functionalities. Many approaches to synthesize helical conjugated polymers have been proposed. Helical polyacetylene (H-PA) films, having helical chains and fibrils, have been synthesized through the polymerization of acetylene in an asymmetric reaction field constructed with N*-LC and Ziegler–Natta catalyst.[13] The introduction of chiral moieties as side chains is widely used to induce helicity to the main chain of conjugated polymers.[4,5] It was also shown that when chiral dopants are added to the N-LC phase of poly-*p*-phenylene (PPP) with LC side chains, the resulting film exhibits chiroptical activity.[14]

Thermotropic N*-LC systems in conjugated polymers have been widely used for generating CPL.[4,5a,b,e,f,14] On the other hand, it would be appealing to investigate lyotropic N*-LC systems as alternative circularly polarized optical materials for use in optoelectronic devices and displays. The effects of the solvent, solution concentration, and chiral dopant employed on the lyotropic N*-LC system would be of particular interest especially in relation to the helical structure of the LC phase and its chiroptical properties.

Various helical polymers with lyotropic LC behavior such as polyisocyanate,[15a] cellulose derivatives,[15b] deoxyribonucleic acid (DNA),[15c–e] and tobacco mosaic virus (TMV)[15f,g] have been extensively studied. The substitution of two bulky side chains directly into the main chain of polyacetylene leads to disubstituted polyacetylene (diPA) exhibiting fluorescence.[16,18] It was reported that fluorescent diPA adopting a poly(diphenylacetylene) (PDPA) structure with alkyl side chains exhibits lyotropic LC behavior.[17,18] The PDPA structure, with phenyl moieties directly attached to the main chain, has a stiff main chain that acts as a LC mesogen, which will self-assemble into a lyotropic LC phase above a critical concentration.

Investigations on the lyotropic LC behavior of PDPAs have been published; however, there are only a small number of reports of PDPAs exhibiting the lyotropic N*-LC phase.[17c] Therefore, examining the lyotropic N*-LC of diPA is worthwhile because it has been shown that N*-LC materials demonstrate supramolecular helical ordering that leads to CPL with high g_{em} and that lyotropic liquid crystallinity has excellent potential for use in CPL devices. For these reasons, we aim to synthesize disubstituted liquid crystalline polyacetylene (diLC-PA) having a lyotropic N*-LC phase to generate CPL with high g_{em}.

In this research, various diLCPA derivatives having either a poly(alkylphenylacetylene) (PAPA) structure or a PDPA main chain structure were synthesized. Chirality in diLCPA was induced by means of substitution of chiral moieties to the side chains or with the use of chiral dopants. The structural effects on the functionalities of the diLCPA derivatives were examined. We focused on the thermotropic and lyotropic LC of the diLCPAs, as well as their photoluminescent (PL), chiroptical, and CPL properties.

In this study, we demonstrate that chiral diLCPA derivatives form a lyotropic N*-LC film, and they exhibit CPL having a high g_{em} value. To the best of our knowledge, the g_{em} values on the order of 10^{-1} are the highest values of CPL achieved in the aliphatic conjugated polymers. In this work, we have found that the highly ordered lyotropic N*-LC phase is essential for the generation of CPL with high g_{em} values.

2. RESULTS AND DISCUSSION

2.1. Synthesis and Characterization of Polymers.

Various disubstituted LCPA derivatives and chiral dopants were synthesized (Scheme 1). The three diLCPA derivatives have a 4-nonyloxy phenyl groups with either racemic (*rac*)-, (*R*)-, or (*S*)- handedness. **PA1** has a poly(alkylphenylacetylene) (PAPA) structure, while **PA2** and **PA3** have a poly(diphenylacetylene) (PDPA) structure that is responsible for both green fluorescence and lyotropic liquid crystallinity. Axially chiral dopants were synthesized as described in a previous report.[13] **(*R*)-/(*S*)-2,2′-PCH506-Binaphthyl**, abbreviated as **(*R*)-/(*S*)-D1**, have phenylcyclohexyl (PCH) LC moieties that are substituted at the 2,2′ position of the binaphthyl rings. The substituted PCH LC moieties of **(*R*)-/(*S*)-D1** improve the miscibility between the polymer and the chiral dopant and also give rise to the chiral induction between them.

Scheme 1. Structures of the Disubstituted LCPA Derivatives and Chiral Dopants

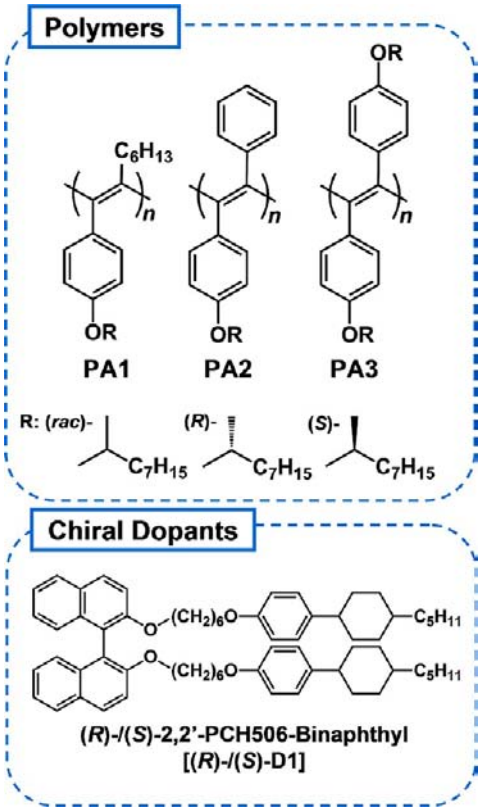

The synthesis routes for the monomers and polymers are shown in Scheme 2. The monomers of the diLCPA derivatives and the chiral dopants were synthesized using chemical reactions, such as Sonogashira–Hagihara coupling,[19a,b] Mitsunobu reaction,[19c] and Williamson etherification reaction.[19d] The monomers were polymerized via a metathesis reaction using tungsten hexachloride (WCl_6) as a catalyst with tetraphenyltin (Ph_4Sn) as a co-catalyst. The polymerization reaction was conducted at 80 °C under an argon atmosphere using toluene as a solvent. The polymerization proceeded for 24 h followed by washing of the polymer in methanol (MeOH) under constant stirring for 24 h. The precipitated polymers were subsequently dried under a vacuum.

dx.doi.org/10.1021/ja3086565 | J. Am. Chem. Soc. 2012, 134, 19795–19807

Scheme 2. Synthesis Routes for the Monomers and Disubstituted LCPA Derivatives[a]

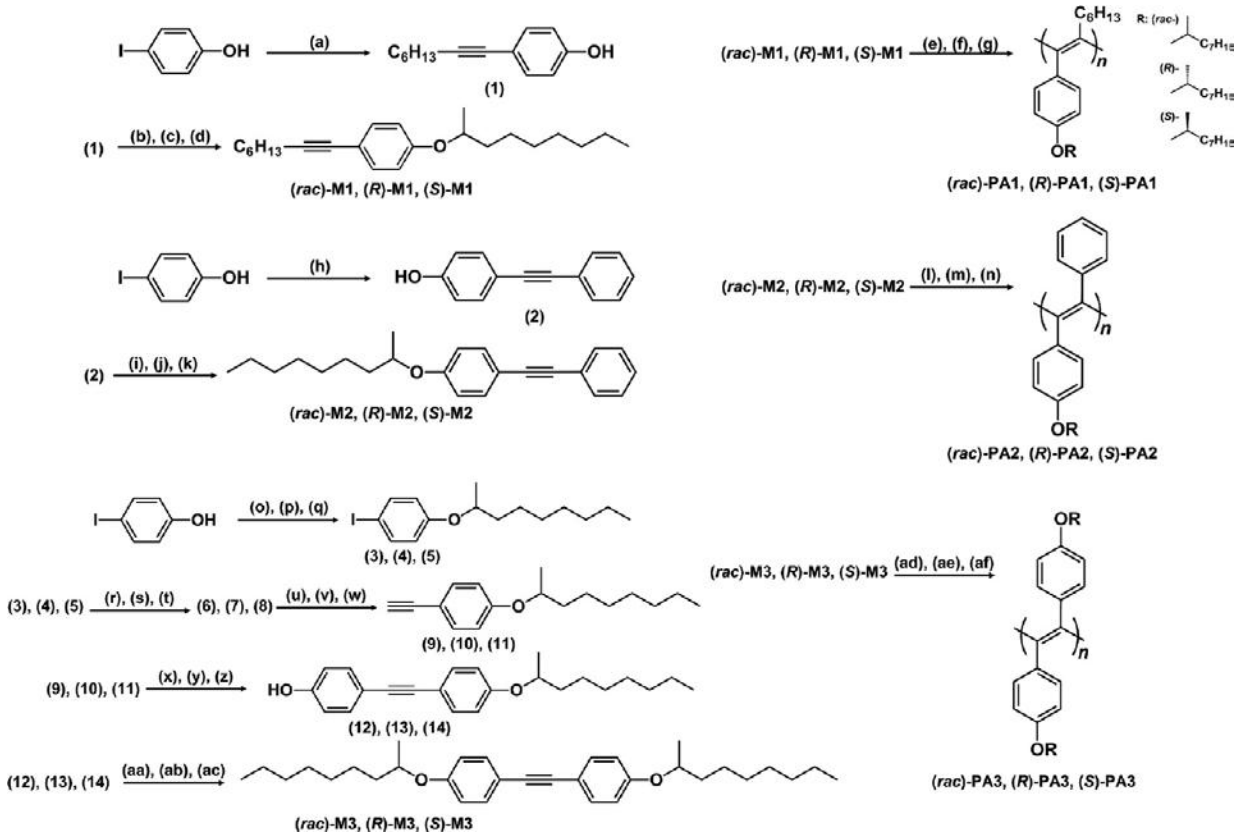

[a]Reagents and conditions: **PA1:** (a) 1-octyne, $PdCl_2(TPP)_2$, CuI, NH_3 (aq), THF, r.t., 24 h; (b,c,d) **1**, (*rac*)/(*S*)/(*R*)-2-nonanol, DEAD, TPP, THF, r.t., 24 h; (e,f,g) (***rac***)**-M1**, (***R***)**-M1**, (***S***)**-M1**, WCl_6, Ph_4Sn, toluene, 80 °C, 24 h; **PA2:** (h) phenylacetylene, $PdCl_2(TPP)_2$, CuI, Et_3N, THF, 65 °C, 24 h; (i,j,k) **2**, (*rac*)/(*S*)/(*R*)-2-nonanol, DEAD, TPP, THF, r.t., 24 h; (l,m,n) (***rac***)**-M2**, (***R***)**-M2**, (***S***)**-M2**, WCl_6, Ph_4Sn, toluene, 80 °C, 24 h; **PA3:** (o,p,q) (*rac*)/(*S*)/(*R*)-2-nonanol, DEAD, TPP, THF, r.t., 24 h; (r,s,t) **3**, **4**, **5**, trimethylsilylacetylene, $PdCl_2(TPP)_2$, CuI, Et_3N, THF, 65 °C, 24 h; (u,v,w) **6**, **7**, **8**, K_2CO_3, MeOH, THF, r.t., 24 h; (x,y,z) **9**, **10**, **11**, 4-iodophenol, $PdCl_2(TPP)_2$, CuI, Et_3N, THF, 65 °C, 24 h; (aa,ab,ac) **12**, **13**, **14**, (*rac*)/(*S*)/(*R*)-2-nonanol, DEAD, TPP, THF, r.t., 24 h; (ad,ae,af) (***rac***)**-M3**, (***R***)**-M3**, (***S***)**-M3**, WCl_6, Ph_4Sn, toluene, 80 °C, 24 h.

The number-average molecular weight (M_n) and the polydispersity (M_w/M_n) of the polymers were measured using gel permeation chromatography (GPC) and calibrated using a polystyrene (PS) standard. The GPC results showed that the polymers have M_n values ranging from 12 700 to 48 300 and M_w/M_n values ranging from 1.7 to 2.8 (Table 1).

2.2. Liquid Crystallinity. The diLCPAs exhibited lyotropic and thermotropic liquid crystallinity. **PA1** exhibited thermotropic LC behavior having a smectic A (S_A) LC phase (see Supporting Information, Figure S1), while **PA2** and **PA3** showed main chain type lyotropic LC behavior. In the case of the **PA1**, the alternating phenyl moieties attached at the polymer main chain act as LC mesogens, and **PA1** shows side chain type liquid crystallinity arranged in a layered S_A phase. Even with the presence of chiral moieties in the side chain of (***R***)-/(***S***)**-PA1**, the side chain type liquid crystalline behavior of **PA1** aligns the main chain into a layered S_A LC phase.

Table 1. Weight-Average (M_w) and Number-Average (M_n) Molecular Weights, Dispersion Degree (M_w/M_n), and Degree of Polymerization (DP) of the Disubstituted LCPAs

	M_w	M_n	M_w/M_n	DP
(*rac*)-**PA1**	100 000	48 300	2.1	151
(*R*)-**PA1**	46 400	26 700	1.7	83
(*S*)-**PA1**	73 500	44 400	1.7	139
(*rac*)-**PA2**	53 000	22 000	2.4	70
(*R*)-**PA2**	53 000	23 000	2.1	72
(*S*)-**PA2**	56 000	25 000	2.3	77
(*rac*)-**PA3**	27 100	13 400	2.0	29
(*R*)-**PA3**	21 000	12 700	2.8	16
(*S*)-**PA3**	33 000	14 000	2.3	30

Previously, we observed main chain type lyotropic LC behavior in diLCPAs having a PDPA structure, which showed a lyotropic nematic LC (N-LC) phase.[18] The main chains of **PA2** and **PA3** have a stiff polymer structure because their side chains are composed of phenyl moieties directly attached to the main chain forming a stilbene fragment enforced by π-conjugation. A polymer exhibiting this elevated level of stiffness should be infusible upon the heating, resulting in an LC with no thermotropic behavior. Instead, by virtue of the nonyloxy group substituted at the phenyl moiety, **PA2** and **PA3** are soluble in organic solvents, such as a toluene, and show lyotropic LC behavior. Note that **PA1** is also soluble in organic solvents, but it shows no lyotropic LC. This finding is probably due to its higher solubility, which might depress the formation of spontaneously aligned self-assemblies that is a prerequisite to the formation of domains of lyotropic LC. In other words, polymers with high solubility are freely dissolved in a solvent with randomly oriented conformation and form neither a regularly stacked nor an associated structure. This situation is

dx.doi.org/10.1021/ja3086565 | J. Am. Chem. Soc. 2012, 134, 19795−19807

far from what is necessary for the formation of the lyotropic LC. In the case of the PDPA structure of **PA2** and **PA3**, the stilbene fragment might be suitable for the formation of an interchain π-electron overlapped association through van der Waals interactions, which enables the polymers to exhibit the lyotropic LC.

In the lyotropic LC phase of (*S*)-**PA2**, the polymer main chains act as LC mesogens, which spontaneously align to form a helically twisted structure in a N*-LC phase. Polarizing optical microscopy (POM) analysis reveals a lyotropic N*-LC phase prepared from 10 wt% solution using toluene as solvent (Figure 1a). Figure 1a shows a double-spiraled texture

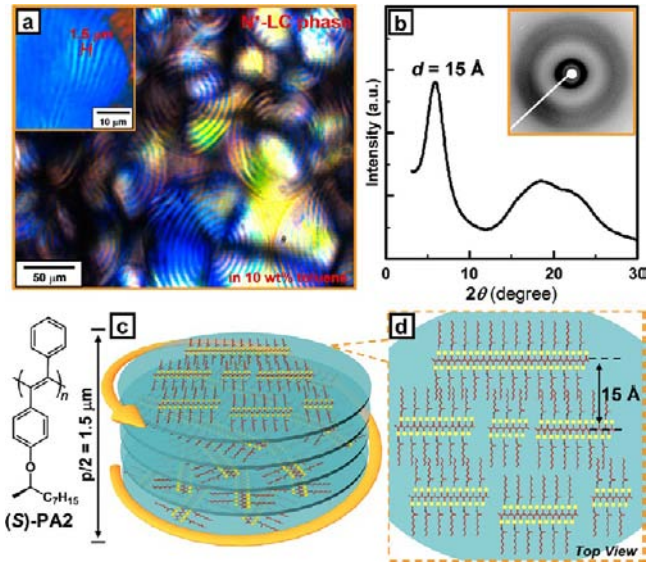

Figure 1. (a) POM image of the N*-LC phase of (*S*)-**PA2** in 10 wt% lyotropic LC solution in toluene showing a double-spiraled texture. Inset shows a fingerprint texture with a half helical pitch of 1.5 μm. (b) XRD pattern of (*S*)-**PA2** shows a reflection at 15.0 Å (5.9° in 2θ) describing the polymer interchain distance within a N*-LC domain. Inset shows the Laue pattern of (*S*)-**PA2**. (c) Schematic representation of the N*-LC phase of (*S*)-**PA2**. (d) Top view of a N*-LC domain describing the polymer interchain distance.

characteristic of the N*-LC phase.[20] The inset of Figure 1a shows a fingerprint texture with a distance of 1.5 μm between striae, which corresponds to the half helical pitch of the N*-LC phase. We performed X-ray diffraction (XRD) on the N*-LC film of (*S*)-**PA2**. The XRD profile of the (*S*)-**PA2** N*-LC film (Figure 1b) shows a peak corresponding to a distance of 15.0 Å, which is assigned as the polymer interchain distance within a N*-LC domain (Figure 1d).[21] The XRD pattern also shows a broad scattering signal in the wide angle range from 15 to 25° (4−6 Å) due to the distance between side chains and/or π-stacking of phenyl rings in the side chain, similar to previous reports of PDPA showing lyotropic LC.[17a,b] Figure 1c shows a schematic representation of the N*-LC phase of (*S*)-**PA2**.

In Figure 2, the chiral induction of (*rac*)-**PA2** forming a N*-LC phase is illustrated. The POM image of (*rac*)-**PA2** shows a Schlieren texture characteristic of lyotropic N-LC phase[20] prepared from 10 wt% toluene solution (Figure 2a). Upon addition of chiral dopant (*S*)-**D1** at 10 wt%, the N-LC phase of (*rac*)-**PA2** changes into a N*-LC phase (Figure 2b). The POM image of (*S*)-**D1**/(*rac*)-**PA2** reveals a fingerprint texture with a half helical pitch of 2.0 μm.[22] XRD analysis on the N-LC film of (*rac*)-**PA2** and N*-LC film of (*S*)-**D1**/(*rac*)-**PA2** (Figure S2) showed XRD profiles similar to (*S*)-**PA2** (Figure 1b).[21]

Table 2 summarizes the LC phases of the diLCPAs. **PA1**, having a PAPA structure, exhibited a thermotropic S_A phase. **PA2** and **PA3** demonstrate lyotropic liquid crystallinity at a critical concentration range from 5 to 10 wt% in toluene. Analogous to thermotropic LCs which show an isotropic phase above a critical temperature, lyotropic LCs become isotropic liquids below 5 wt% concentration in toluene, where the polymer main chains (which act as LC mesogens) are dispersed randomly without any ordering. At the lyotropic LC concentration range, there are weak π-interactions between the aromatic stilbene structure and toluene. In such a situation, the toluene enhances the attraction between polymer main chains for spontaneous self-assembly to occur and also provide enough fluidity in the system for liquid crystallinity to take place.

(*rac*)-**PA2** and (*rac*)-**PA3** displayed a lyotropic N-LC phase, while (*R*)-/(*S*)-**PA2** (Figure 1a) and (*R*)-/(*S*)-**PA3** (Figure S3a) exhibited a lyotropic N*-LC phase. **D1**-doped (*rac*)-**PA2** (Figure 2b) and **D1**-doped (*rac*)-**PA3** (Figure S3b) also exhibited a N*-LC phase through chiral induction. Thus, by introducing chirality to diLCPA, either with a chiral moiety on the side chain or with the addition of a chiral dopant, a lyotropic N*-LC phase was formed in diLCPA, as long as the PDPA structure is adopted in the polymer main chain.

2.3. Absorption and Photoluminescence. In the case of polymer solutions in a good solvent such as chloroform ($CHCl_3$), the high solubility of the polymer main chains in the solvent depresses the spontaneous self-assembly required for liquid crystallinity to occur. To investigate the optical properties of the diLCPAs in an isotropic state, we prepared the diLCPA solutions using $CHCl_3$ in a concentration of 1.2×10^{-4} M. We examined the UV−vis, PL, absolute fluorescence quantum yield (Φ), and specific rotation ($[\alpha]_D$) of the diLCPAs in isotropic solution ($CHCl_3$) and as cast films (Table 3).

PA1 exhibits a main chain absorption band measuring ~340 nm and a blue-colored emission measuring ~450 nm in both solution and film (Figure 3a). Conversely, **PA2** and **PA3** show a main chain absorption band of ~440 nm and a *trans*-stilbene moiety-based absorption band measuring ~380 nm. **PA2** and **PA3** display a green colored emission of ~500 nm in both solution and film (Figure 3b,c). Previously, we elucidated the origin of emission of substituted PAs and investigated the fluorescent trends of diLCPA.[18] In that earlier work, we observed that diLCPAs with PAPA and PDPA structures generally exhibit blue and green emissions, respectively. The green emission color of the latter is associated with the PDPA structure in which two bulky phenyl rings are directly attached to the polyene main chain. Specifically, the two bulky side chains contribute to lower the $1B_u$ excited state and later to decrease the band gap,[23] resulting in a bathochromic shift of the **PA2** and **PA3** emission bands. Generally, the PAs show small emission shifts between the solution and cast film, which is advantageous for applications of diLCPAs as fluorescent materials in EL devices. Absolute fluorescence quantum yields (Φ) of the diLCPAs in solution and in cast film were measured using the integrating-sphere method. The quantum yields of the diLCPAs in solution range from 21 to 34%, while those in cast film from 10 to 14%. Specific rotation ($[\alpha]_D$) measurements showed that (*R*)-/(*S*)-**PA3** (~±2100°) have values an

dx.doi.org/10.1021/ja3086565 | J. Am. Chem. Soc. 2012, 134, 19795−19807

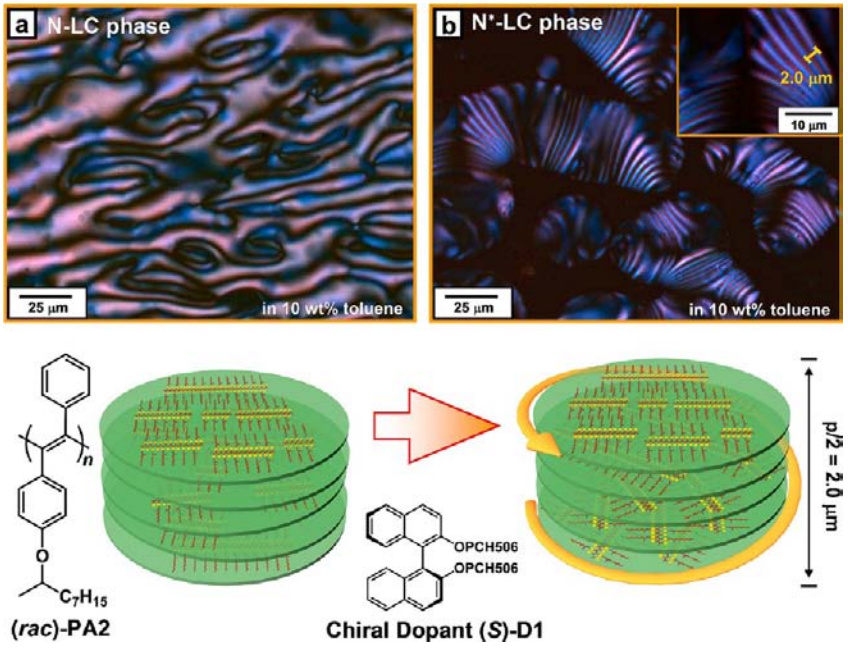

Figure 2. Schematic model of the chiral induction of (*rac*)-**PA2** into a N*-LC phase. Upon the addition of the chiral dopant (*S*)-**D1** at 10 wt% into the N-LC phase of (*rac*)-**PA2** (left), a N*-LC phase is induced (right). (a) POM image of the N-LC phase of (*rac*)-**PA2** 10 wt% lyotropic LC solution in toluene showing a Schlieren texture. (b) POM image of the N*-LC phase of (*S*)-**D1**/(*rac*)-**PA2** in 10 wt% lyotropic LC solution in toluene showing a fingerprint texture. Inset shows the half helical pitch of 2.0 μm.

Table 2. Thermotropic and Lyotropic Liquid Crystallinity of the Disubstituted LCPAs[a]

Polymers		LC phase	
(*rac*)-	PA1	Thermotropic	G 95 S_A over G 65 S_A 300
(*R*)-/(*S*)-	PA1	Thermotropic	
(*rac*)-	PA2	Lyotropic	N (5–10wt % in toluene)
(*R*)-/(*S*)-	PA2	Lyotropic	N* (5–10wt % in toluene)
(*rac*)-	PA3	Lyotropic	N (5–10wt % in toluene)
(*R*)-/(*S*)-	PA3	Lyotropic	N* (5–10wt % in toluene)
(*R*)-/(*S*)-D1	(*rac*)-PA2	Lyotropic	N* (5–10wt % in toluene)
(*R*)-/(*S*)-D1	(*rac*)-PA3	Lyotropic	N* (5–10wt % in toluene)

[a]Red, heating process; blue, cooling process; G, glassy state; N, nematic; N*, chiral nematic; S_A, smectic A.

order of magnitude higher than (*R*)-/(*S*)-**PA1** (~±240°) and (*R*)-/(*S*)-**PA2** (~±220°).

2.4. Circular Dichroism. With the aim to investigate the helical conformation and arrangement of the polymer chains in an isotropic, aggregate, and liquid crystalline self-assembled state, we measured the circular dichroism (CD) spectra of the diLCPA derivatives in $CHCl_3$ solution, cast film, and N*-LC film.

Solutions of the diLCPAs were prepared using $CHCl_3$ (c = 1.2×10^{-4} M) as solvent. The cast film samples were prepared by dissolving the diLCPAs in $CHCl_3$, and later casting the solution onto a quartz plate. The N*-LC film samples were prepared by dissolving the diLCPAs or the diLCPAs with chiral dopant[24] in toluene (5–10 wt%) to form a lyotropic LC state. The LC solution was subsequently cast onto a quartz plate, which was later exposed under toluene vapor for one hour and was dried slowly at room temperature. Toluene vapor exposure of the N*-LC film was performed to increase the domain size of the N*-LC phase.

The CD spectra of the diLCPAs in $CHCl_3$ solution showed monosignate Cotton effects at the absorption region of the

Table 3. Spectroscopic Data for Absorption (λ_{max}), Fluorescence ($E_{m,max}$), Excitation ($E_{x,max}$), Quantum Yield (Φ), and Specific Rotation ($[\alpha]_D$) of the Disubstituted LCPAs in $CHCl_3$ and Film

	λ_{max} (nm)		$E_{m,max}$ (nm)		$E_{x,max}$ (nm)		Φ (%)[a]		$[\alpha]_D$ (deg)[b]
	in $CHCl_3$	film	in $CHCl_3$	film	in $CHCl_3$	film	in $CHCl_3$	film	in $CHCl_3$
(*rac*)-**PA1**	340	340	454	444	337	340	26	12	N/A
(*R*)-**PA1**	338	338	452	444	338	338	21	10	−241
(*S*)-**PA1**	344	341	452	445	336	341	22	11	+247
(*rac*)-**PA2**	430	428	501	502	361	374	29	11	N/A
(*R*)-**PA2**	430	430	502	500	376	378	24	14	+229
(*S*)-**PA2**	432	428	501	501	365	374	28	13	−226
(*rac*)-**PA3**	438	438	501	494	372	365	34	13	N/A
(*R*)-**PA3**	440	444	501	493	372	365	29	12	+2080
(*S*)-**PA3**	436	438	498	493	372	365	33	13	−2158

[a]Absolute quantum yield measured using integrating-sphere method. [b]Specific rotation measured at room temperature in chloroform.

dx.doi.org/10.1021/ja3086565 | *J. Am. Chem. Soc.* 2012, 134, 19795–19807

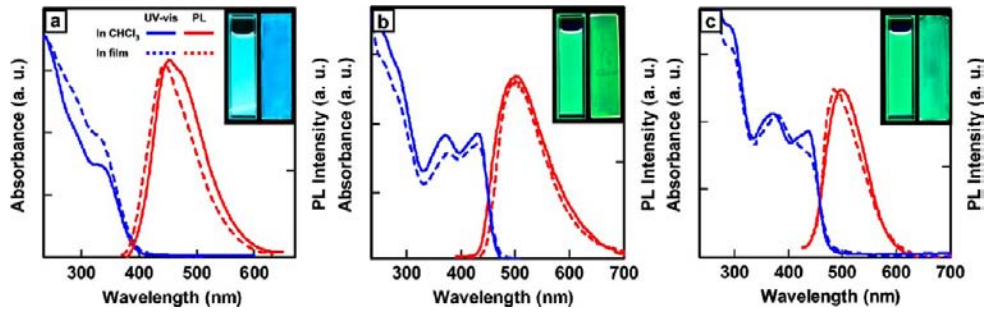

Figure 3. UV−vis and PL spectra of (a) (*R*)-**PA1**, (b) (*R*)-**PA2**, (c) (*R*)-**PA3** in $CHCl_3$ solution ($c = 1.2 \times 10^{-4}$ M) and in cast film. Insets: PLs in $CHCl_3$ solution (left) and in cast film (right).

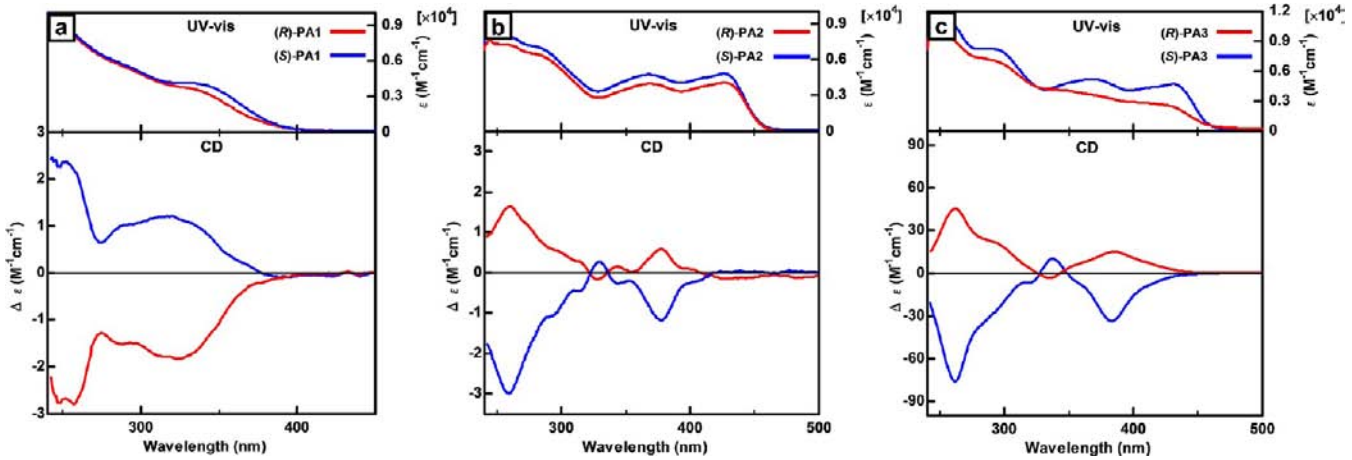

Figure 4. UV−vis (upper) and CD spectra (lower) in $CHCl_3$ solution ($c = 1.2 \times 10^{-4}$ M) of (a) (*R*)-/(*S*)-**PA1**, (b) (*R*)-/(*S*)-**PA2**, and (c) (*R*)-/(*S*)-**PA3**.

polymer main chains (Figure 4a−c).[25] These results imply that the diLCPAs have a one-handed helical excess conformation. The monosignate Cotton effects of the CD spectra of the diLCPAs suggest intrachain helicity of the polyene main chains. The degree of CD was evaluated using absorption dissymmetry factor, g_{abs}. This factor is defined by the following equation: $g_{abs} = (\varepsilon_L - \varepsilon_R)/[(\varepsilon_L + \varepsilon_R)/2] = \Delta\varepsilon/\varepsilon$, where $|g_{abs}| < 2$. The ε_L and ε_R are defined as the absorption coefficients of left- and right-handed polarized light, respectively. The CD spectra of (*R*)-/(*S*)-**PA1** and (*R*)-/(*S*)-**PA2** in solution showed g_{abs} values on the order of 10^{-4}, while (*R*)-/(*S*)-**PA3** showed g_{abs} values on the order of 10^{-3} (Table 4), which suggest that (*R*)-/(*S*)-**PA3** in solution may have a more strongly twisted main chain helical conformation compared to (*R*)-/(*S*)-**PA1** and (*R*)-/(*S*)-**PA2**. The two chiral nonyloxy moieties in (*R*)-/(*S*)-**PA3** induce a stronger helical conformation to the main chain, as quantified by $\Delta\varepsilon$ and g_{abs} values observed in the CD spectra in solution. The measured specific rotation values of the diLCPAs in solution (Table 3) also support the CD results, where (*R*)-**PA3** (+2,080°) and (*S*)-**PA3** (−2,158°) showed values an order higher than (*R*)-**PA1** (−241°), (*S*)-**PA1** (+247°), (*R*)-**PA2** (+229°), and (*S*)-**PA2** (−226°).

Table 4. Absorption Dissymmetry Factors (g_{abs}) of the Disubstituted LCPAs in $CHCl_3$ Solution, Cast Film, and N*-LC Film

	g_{abs} (wavelength/nm)[a]	
	$CHCl_3$	cast film/N*-LC film
(*R*)-**PA1**	-8.3×10^{-4} (325)	-6.8×10^{-4} (326)[b]
(*S*)-**PA1**	4.9×10^{-4} (320)	5.9×10^{-4} (326)[b]
(*R*)-**PA2**	1.5×10^{-4} (378)	1.7×10^{-1} (455)[c]
(*S*)-**PA2**	-2.6×10^{-4} (378)	-1.3×10^{-1} (445)[c]
(*R*)-**PA3**	4.8×10^{-3} (388)	-2.9×10^{-2} (453)[c]
(*S*)-**PA3**	-7.3×10^{-3} (385)	5.4×10^{-2} (451)[c]
(*R*)-**D1**/(*rac*)-**PA2**	N/A	-4.2×10^{-2} (449)[c]
(*S*)-**D1**/(*rac*)-**PA2**	N/A	6.1×10^{-2} (459)[c]

[a]Wavelength at which g_{abs} was evaluated. [b]In cast film. [c]In N*-LC film.

Cast films of (*R*)-/(*S*)-**PA1** showed monosignate Cotton effects in the absorption region of the polymer main chain (Figure 5a). For the other samples, the CD spectra of (*R*)-/(*S*)-**PA2** and (*R*)-/(*S*)-**PA3** in cast film and in N*-LC film exhibited bisignate Cotton effects in the absorption region of the polymer main chain.[26] Using the exciton coupling theory,[27] we can deduce that (*R*)-/(*S*)-**PA2** and (*R*)-/(*S*)-**PA3** have interchain helical π-stacking between the polymer main chains. (*R*)-**PA2**, which has a positive and negative Cotton effect at longer wavelengths and shorter wavelengths, respectively, can be assigned as having *P*-helicity with a right-handed (clockwise) π-stacked structure, while (*S*)-**PA2** can be assigned as having *M*-helicity with a left-handed (counterclockwise) π-stacked structure (Figure 5b). From the CD spectra, (*R*)-**PA3** and (*S*)-**PA3** are assigned as having *M*-helicity and *P*-helicity, respectively (Figure 5c). The cast films of (*R*)-/(*S*)-**PA2** and (*R*)-/(*S*)-**PA3** exhibited similar CD spectra and handedness to the **PA2** and **PA3** N*-LC samples (Figure S5a,b). It should be noted that the CD spectra of (*R*)-/(*S*)-**PA1** in cast film form showed no bisignate CD signal in the polymer main chain absorption region. These results suggest that the PDPA

dx.doi.org/10.1021/ja3086565 | J. Am. Chem. Soc. 2012, 134, 19795−19807

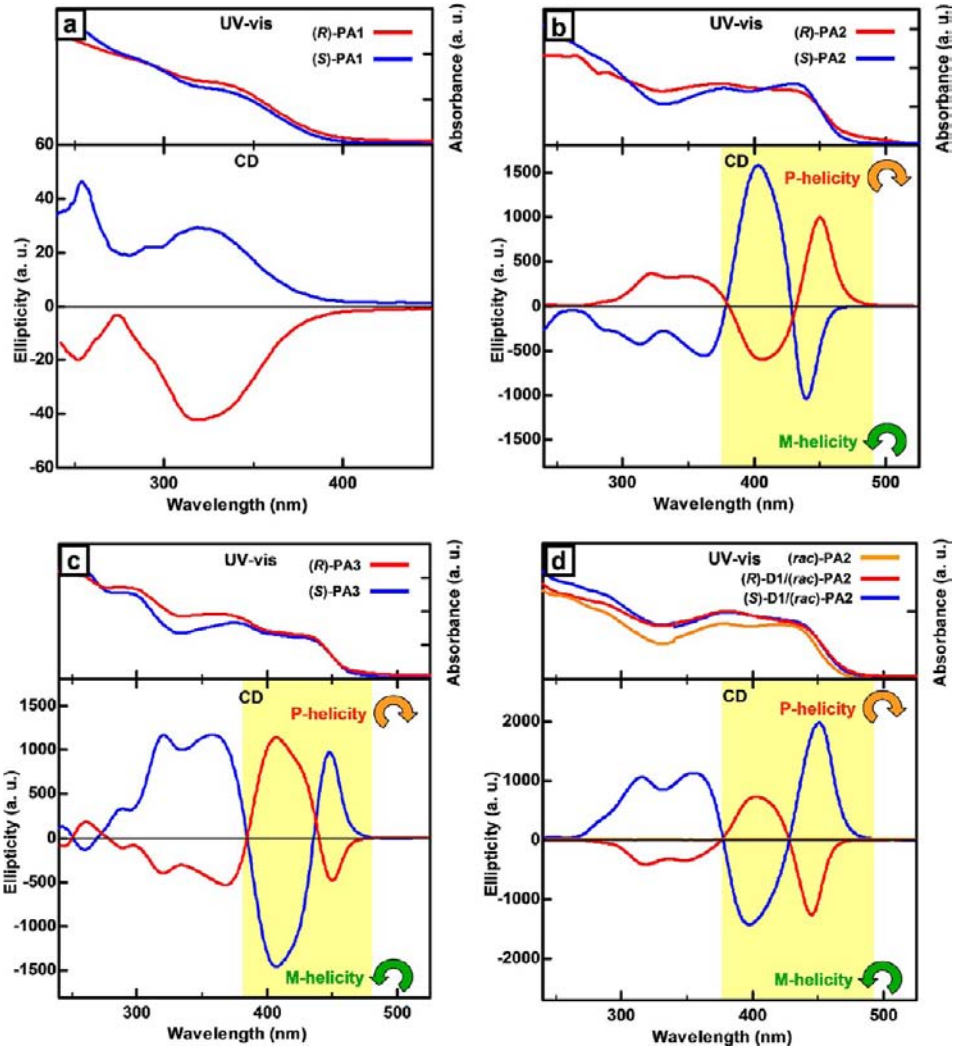

Figure 5. UV−vis (upper) and CD spectra (lower) of (a) (*R*)-/(*S*)-**PA1** cast film, and (b) (*R*)-/(*S*)-**PA2** N*-LC film, (c) (*R*)-/(*S*)-**PA3** N*-LC film, (d) (*R*)-/(*S*)-**D1** doped (*rac*)-**PA2** (10 wt%) N*-LC film.

structure of (*R*)-/(*S*)-**PA2** and (*R*)-/(*S*)-**PA3** facilitates helical π-stacking in cast film and N*-LC state.

It should be noted that (*R*)-**PA2** and (*R*)-**PA3**, having the same configuration of chiral moieties, exhibit the same intrachain helical sense in solution (Figure 4b,c, Table 4). However, in cast films and N*-LC films, (*R*)-**PA2** and (*R*)-**PA3** exhibit opposite bisignate Cotton effects with *P*- and *M*-helicity, respectively (Figure 5b,c, Table 4). Such behavior may be related to the chiral organization of the polymer main chains during self-assembly from a disordered (solution) state to a helical π-stacked structure in cast film and N*-LC states. The degree of the attractive interchain π-stacking interactions during self-assembly would be quite different for (*R*)-**PA2** and (*R*)-**PA3** because the latter has a more twisted helical main chain conformation induced by its two chiral nonyloxy moieties. Such a difference in attractive π-stacking interactions would be sufficient to favor a different helical sense during the self-assembly of (*R*)-**PA2** and (*R*)-**PA3**.

D1-doped (*rac*)-**PA2** N*-LC films exhibited bisignate Cotton effects at the polymer main chain region. It was observed that (*R*)-**D1**/(*rac*)-**PA2** N*-LC film showed *M*-helicity, while (*S*)-**D1**/(*rac*)-**PA2** N*-LC film showed *P*-helicity (Figure 5d). The CD spectra of (*rac*)-**PA2** displayed no optical handedness; therefore, the chirality of **D1**-doped (*rac*)-**PA2** originated from the chiral induction of the (*rac*)-**PA2**. Moreover, **D1**-doped (*rac*)-**PA3** in N*-LC film also showed a bisignate CD spectra (Figure S5c).

It is also interesting that (*R*)-**PA2** and (*R*)-**D1**/(*rac*)-**PA2** N*-LC films showed bisignate Cotton effects with *P*- and *M*-helicity, respectively (Figure 5b,d, Table 4). The chiral organization of these two N*-LC films during self-assembly would be quite different because the chirality of (*R*)-**PA2** and (*R*)-**D1** exhibits central chirality and axial chirality, respectively. Similarly, differences in the type of chirality would be sufficient to favor a different helical sense during the self-assembly of (*R*)-**PA2** and (*R*)-**D1**/(*rac*)-**PA2** N*-LC films. (*R*)-**PA3** (Figure 5c) and (*R*)-**D1**/(*rac*)-**PA3** (Figure S5c) films also exhibit opposite helical sense in helical π-stacking.

(*R*)-/(*S*)-**PA1** in cast film form showed g_{abs} values on the order of 10^{-4}, and (*R*)-/(*S*)-**PA3** and **D1**-doped (*rac*)-**PA2** N*-LC films showed g_{abs} values on the order of 10^{-2}, while (*R*)-/(*S*)-**PA2** N*-LC films showed g_{abs} values up to 10^{-1} (Table 4).[28] It can be observed that the g_{abs} values of the (*R*)-/(*S*)-**PA2** and (*R*)-/(*S*)-**PA3** cast films are an order smaller than those of (*R*)-/(*S*)-**PA2** and (*R*)-/(*S*)-**PA3** N*-LC films (Table S1).

The CD spectra of the diLCPAs indicate that one-handed intrachain helical structure is formed in solution, while the

dx.doi.org/10.1021/ja3086565 | J. Am. Chem. Soc. 2012, 134, 19795−19807

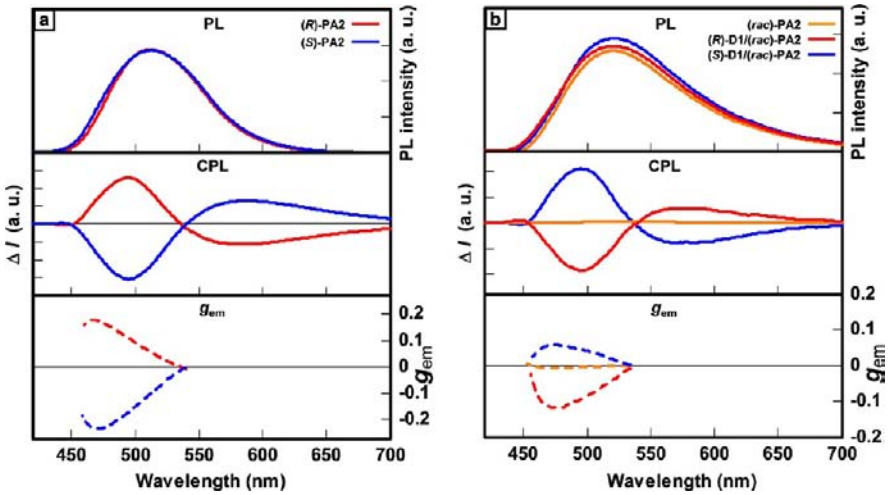

Figure 6. PL (upper), CPL spectra (middle), and g_{em} (lower) spectra of (a) (*R*)-/(*S*)-**PA2** N*-LC film, and (b) (*R*)-/(*S*)-**D1**-doped (*rac*)-**PA2** (10 wt%) N*-LC film. The measurements were performed with excitation using unpolarized light at 367 nm.

interchain helical π-stacking between the polymer main chains is formed in cast films and in N*-LC films. The diLCPAs in solution showed g_{abs} values up to the orders of 10^{-3}, while diLCPAs in N*-LC film are in orders of up to 10^{-1}. These results indicate that an increase in interchain interactions from solution to cast film and a subsequently further increase in N*-LC film, leading to a higher degree of helical π-stacked ordering.

2.5. Circularly Polarized Luminescence. We investigated the potential of circularly polarized luminescence (CPL) of the diLCPAs. Even though the diLCPAs in solution and in cast film showed Cotton effects in their CD spectra, they exhibited no CPL.

However, (*R*)-/(*S*)-**PA2** in N*-LC film showed bisignate CPL bands centered around the PL emission band (Figure 6a). (*R*)-**PA2** bearing *P*-helicity in the π-stacked structure exhibited positive and negative CPL bands at wavelengths shorter and longer than 530 nm, respectively. (*S*)-**PA2**, which has *M*-helicity in the π-stacked structure, exhibited CPL bands with handedness opposite to (*R*)-**PA2**. The degree of CPL was evaluated by the emission dissymmetry factor, g_{em}. The emission dissymmetry factor is defined as $g_{em} = (I_L - I_R)/[(I_L + I_R)/2] = \Delta I/I$, where $|g_{em}| < 2$. The I_L and I_R are defined as the intensities of left- and right-handed polarized light, respectively. The CPL spectra of (*R*)-/(*S*)-**PA2** in N*-LC film showed g_{em} values up to orders of 10^{-1} (Table 5).[28] These high g_{em} values suggest the formation of higher ordered helical π-stacked structures in the N*-LC film of (*R*)-/(*S*)-**PA2**. The g_{em} values on the order of 10^{-1} are the highest values of CPL achieved in the aliphatic conjugated polymers to the best of our knowledge.

Table 5. Emission Dissymmetry Factors (g_{em}) of the Disubstituted LCPAs in N*-LC Films

	g_{em}(wavelength/nm)[a]
(*R*)-**PA2**	1.8×10^{-1} (466)
(*S*)-**PA2**	-2.3×10^{-1} (471)
(*R*)-**D1**/(*rac*)-**PA2**	-1.2×10^{-1} (478)
(*S*)-**D1**/(*rac*)-**PA2**	5.9×10^{-2} (473)

[a]Wavelength at which g_{em} was evaluated.

The N*-LC film of **D1**-doped (*rac*)-**PA2** exhibited CPL similar to that of (*R*)-/(*S*)-**PA2** (Figure 6b). The CPL spectra of **D1**-doped **PA2** films show handedness opposite to their counterparts in (*R*)-/(*S*)-**PA2** with g_{em} values up to orders of 10^{-1}. The CPL spectrum of (*rac*)-**PA2** showed no CPL; therefore, the CPL of **D1**-doped (*rac*)-**PA2** originated from the chiral induction of the (*rac*)-**PA2**. (*R*)-/(*S*)-**PA3** and **D1**-doped (*rac*)-**PA3** N*-LC films also exhibited CPL (Figure S6, Table S2).

It should be noted that (*R*)-**PA2** and (*R*)-**D1**/(*rac*)-**PA2** N*-LC films, which showed *P*- and *M*- helicity, respectively, in their helical π-stacked structure, also exhibited g_{em} values with opposite signs. The same trend of opposite signs in the g_{abs} and g_{em} values was also observed in (*R*)-**PA2** and (*R*)-**PA3**. This finding suggests that the chiral organization of the helically π-stacked structures influences the CPL behavior of the diLCPAs.

In contrast to **PA2** and **PA3**, (*R*)-/(*S*)-**PA1**, bearing a PAPA main chain structure, exhibited no CPL in cast films. These results, along with the CD data, suggest that the PDPA main chain structure is much more suitable for the helical π-stacking necessary for CPL in diLCPA. Furthermore, the lyotropic LC properties of the PDPA main chain enables the formation of a higher-ordered helical arrangement through the N*-LC phase that is essential for the emergence of CPL with high values of g_{em}.

2.6. Relationships between Helical Arrangement, Interchain Interaction, and *g*-Factors of diLCPAs. At this stage, it is helpful to summarize the relationships between helical arrangement, interchain interaction and *g*-factors of diLCPAs, as represented by (*R*)-**PA2**, depicted in Table 6. The relationship between the degree of helical arrangement and the magnitude of interchain interactions of the diLCPAs can be elucidated by comparing the measured *g*-factors in CD and CPL at different states. In the case of (*R*)-**PA2** in $CHCl_3$ solution, we observed intrachain helicity with weak interchain interactions. The CD spectrum of (*R*)-**PA2** in solution revealed monosignate Cotton effects with g_{abs} values on the order of 10^{-4}. On the other hand, in the cast film of (*R*)-**PA2**, the interchain interactions are large enough to give interchain helical π-stacking. The emergence of a bisignate Cotton effect in CD spectra with g_{abs} values up to orders of 10^{-2} indicates that the helical π-stacking between polymer main chains is

dx.doi.org/10.1021/ja3086565 | J. Am. Chem. Soc. 2012, 134, 19795−19807

Table 6. Summary of the Relationship between Helical Arrangement, Interchain Interaction, and *g*-Factors of (*R*)-PA2 at Various States

	in solution	in cast film	in N*-LC film
helical arrangement	intrachain helicity	interchain π-stacking	higher ordered helical arrangement
interchain interaction	weak	large	very large
g_{abs} of (*R*)-PA2 (λ, nm)[a]	1.5×10^{-4} (378)	3.7×10^{-2} (445)	1.7×10^{-1} (455)
g_{em} of (*R*)-PA2 (λ, nm)[a]			1.8×10^{-1} (466)

[a]Wavelength at which g_{abs} and g_{em} were evaluated.

formed through polymer interchain chiral aggregation. While in the N*-LC state, very large interchain interactions are present, resulting in a highly ordered interchain helical arrangement. The CD and CPL spectra of (*R*)-PA2 in the N*-LC state show high g_{abs} and g_{em} values of up to orders of 10^{-1}, respectively. This trend in the CD and CPL results of the diLCPAs leads us to believe that the use of the N*-LC phase facilitates a high degree of supramolecular helical ordering and is indispensable for the emergence of CPL with high *g*-factors.

As a consequence, when one designs polyacetylene derivatives with CPL having a high g_{em}, it is essential to adopt a PDPA main chain structure, to introduce helicity to the main chain, and to utilize the lyotropic LC behavior of PDPA to form a higher-ordered helical structure through the N*-LC phase.

3. CONCLUSION

We synthesized chiral diLCPA derivatives that show a highly ordered lyotropic N*-LC phase, thereby giving rise to a high degree of circular polarization. The PDPA main chain structure of the diLCPAs, along with chirality induced with either chiral nonyloxy phenyl moieties or chiral dopants, allows the formation of a highly ordered lyotropic N*-LC phase. We found that the highly ordered lyotropic N*-LC phase is indispensable for the generation of CPL with high g_{em} values. In addition to having the highest values of CPL in aliphatic conjugated polymers, our approach represents an attractive alternative to thermotropic LC systems for the development of LC-based optoelectronic devices and future applications that utilize circularly polarized optical materials.

4. EXPERIMENTAL SECTION

4.1. Materials. The chemical reagents we purchased from commercially available sources and were used as received. *trans*-Dichlorobis(triphenylphosphine)palladium(II) ($PdCl_2(TPP)_2$) was purchased from Aldrich Co. Ltd. Diethylazodicarboxylate (DEAD), tetraphenyltin (Ph_4Sn), 1-octyne, 4-iodophenol, trimethylsilylacetylene, and 2-nonanol were purchased from Tokyo Kasei Co. Ltd. Tungsten(VI) hexachloride (WCl_6), and copper(I) iodide (CuI) were purchased from Kanto Chemical Co. Ltd. Triphenylphosphine (TPP), (*R*)-(−)-2-nonanol, (*S*)-(+)-2-nonanol, and 25% ammonia (NH_3) solution were purchased from Wako Co. Ltd. Phenylacetylene, potassium carbonate (K_2CO_3), sodium sulfate (Na_2SO_4), triethyl amine (Et_3N), tetrahydrofuran (THF), toluene, methanol (MeOH), hexane (n-C_6H_{14}), ethyl acetate, and chloroform ($CHCl_3$) were purchased from Nacalai Tesque Co. Ltd. All experiments were performed under argon (>99.9995% purity) atmosphere. THF, Et_3N, and toluene used were distilled from sodium as a drying agent under argon gas before use.

4.2. Methods. Proton (^1H) and carbon (^{13}C) nuclear magnetic resonance (NMR) spectra were measured in chloroform-*d* using either JEOL JNM EX400 400 MHz or JEOL AL-400 400 MHz NMR spectrometer. Chemical shifts are represented in parts per million downfield from tetramethylsilane (TMS) as an internal standard. Elemental analysis was measured using a Yanako CHN Corders (MT-3, MT-5 and MT-6), JSL JM-10, Mitsubishi chemical analytech AQF-100 and Dionex ICS-1500.

The microscope observation was carried out under crossed nicols using a Carl Zeiss Axio Imager M1m polarizing microscope equipped with a Carl Zeiss AxioCam MRc5 digital camera and a Linkam TH600PM and L600 heating and cooling stage with temperature control. The samples for observations with POM were sandwiched between two cover glasses.

Optical absorption spectra were measured using a JASCO V-570 UV/VIS/NIR spectrophotometer, and fluorescence spectra were measured using JASCO FP-750 spectrometer with quartz cell (for solution) and quartz plate (for cast film). Absolute fluorescence quantum yield of the polymers was measured using integrating-sphere method at the JASCO FP-6500 spectrometer. Optical purity of the chiral compounds and polymers were evaluated with specific rotation measured by JASCO P2300 polarimeter. Circular dichroism spectra were measured using JASCO J-820 spectropolarimeter. Circularly polarized luminescence was measured using JASCO CPL-200S spectrometer.

The molecular weights of the polymers were determined by gel permeation chromatography (GPC) using a PLgel 5 μm MIXED-D (Polymer Laboratories), a JASCO MD915 UV detector and THF as an eluent at a flow rate of 1.0 mL/min during measurements, where the instrument was calibrated using polystyrene (PS) standard, and were calculated on an 807-IT integrator.

XRD diffraction (XRD) measurements of the polymers were performed with a Rigaku ultra X18 diffractometer (X-ray Cu Kα radiation: 40 kV/300 mA, λ = 0.154 nm; camera length: 100 mm) and a Rigaku Nanoviewer Micromax-007HF diffractometer (X-ray Cu Kα radiation: 40 kV/30 mA, λ = 0.154 nm; camera length: 120 mm). XRD patterns were recorded with an X-ray generator with Nickel filtered Cu Kα radiation and a flat plate camera (RINT2500, Rigaku). The polymers were heated up to isotropic state, and then slowly cooled to room temperature via LC states, yielding XRD samples. Lyotropic LC samples for XRD measurements were prepared by first dissolving the polymer in toluene (5−10 wt% solution) to form a lyotropic LC phase. The lyotropic LC solution is then pulled up a XRD capillary tube (Hilgenberg Mark-tube glass no. 10, 0.01 mm wall thickness) and allowed to dry, yielding XRD samples. The diffraction pattern was recorded on an imaging plate and scanned by a R-AXIS DS3A imaging plate reader at 100 μm resolution.

4.3. Syntheses of Monomers and Polymers. The synthesis routes for precursor compounds **1** to **14** are detailed in the Supporting Information. The syntheses of the diLCPA monomers (*rac*)-/(*R*)-/(*S*)-**M1**−**M3**, the diLCPAs (*rac*)-/(*R*)-/(*S*)-**PA1**−**PA3** are written below. Synthesis of the chiral dopants (*R*)-/(*S*)-**D1** were synthesized as described in a previous report.[13]

(rac)-Monomer 1 ((rac)-M1). (*rac*)-**M1** was synthesized as follows. Into a 100 mL three-necked flask were added compound **1** (0.81 g, 5.69 mmol) and TPP (1.37 g, 5.22 mmol) under argon gas and dissolved in THF (30 mL). In the addition funnel, a mixture of DEAD (2.64 g, 40 wt% in toluene, 5.22 mmol), 2-nonanol (0.68 g, 4.74 mmol), and 30 mL THF were prepared. After dissolving the reagents under constant stirring, the flask was placed in an ice bath and the THF solution in the addition funnel was added dropwise to the solution in the flask. The solution was left overnight at room temperature. Thin layer chromatography (TLC) indicated completion of the reaction. After evaporation of the solvent, the residue was washed with water and extracted with $CHCl_3$ (3×). The residue was

dx.doi.org/10.1021/ja3086565 | J. Am. Chem. Soc. 2012, 134, 19795−19807

dried over anhydrous Na_2SO_4 and the crude product was then purified by open column chromatography using $CHCl_3$ as eluent. The product was evaporated and dried under vacuum to give 0.78 g (2.37 mmol) of (***rac***)-**M1** as a light yellow oil. Yield = 50%.

Anal. Calcd for $(C_{23}H_{36}O)_n$ (328.53)$_n$: C, 84.09; H, 11.04; O, 4.87, Found: C 83.84, H 10.98. ^{1}H NMR (400 MHz, $CDCl_3$): δ = 0.79–0.98 (m, 6H, $-CH_3$), 1.21–1.48 (m, 18H, Ar–O–CH(CH_3)$(CH_2)_6CH_3$, –C≡C–$(CH_2)_2(CH_2)_3CH_3$), 1.49–1.78 (m, 5H, Ar–O–CH$(CH_3)(CH_2)_6CH_3$, –C≡C–$CH_2CH_2(CH_2)_3CH_3$), 2.38 (t, 2H, J = 7.2 Hz, –C≡C–$CH_2(CH_2)_4CH_3$), 4.28–4.39 (m, 1H, Ar–O–$CH(CH_3)(CH_2)_6CH_3$), 6.78 (d, 2H, J = 8.8 Hz, Ar–H *meta* to C_6H_{13}–C≡C–), 7.30 (d, 2H, J = 9.2 Hz, Ar–H *ortho* to C_6H_{13}–C≡C–). ^{13}C NMR (400 MHz, $CDCl_3$): δ = 14.1, 19.1, 21.9, 22.0, 24.9, 28.0, 28.2, 28.6, 28.9, 30.8, 31.2, 35.8, 73.3, 79.6, 87.9, 114.9, 115.2, 132.1, 156.9. HRMS (DART) calcd for $C_{23}H_{36}O$ [M + H$^+$]: 329.2839. Found: 329.2829.

(R)-Monomer 1 ((R)-M1). (***R***)-**M1** was synthesized in a similar way as (***rac***)-**M1**. Into a 100 mL three-necked flask were added compound **1** (1.05 g, 5.19 mmol) and TPP (1.25 g, 4.76 mmol) under argon gas and dissolved in THF (30 mL). In the addition funnel, a mixture of DEAD (2.41 g, 40 wt% in toluene, 4.75 mmol), (*S*)-(+)-2-nonanol (0.62 g, 4.32 mmol), and 30 mL THF was prepared. The reagents were then stirred overnight at room temperature. The reaction yielded a light yellow oil with a yield of 66% (0.93 g, 2.84 mmol).

Anal. Calcd for $(C_{23}H_{36}O)_n$ (328.53)$_n$: C, 84.09; H, 11.04; O, 4.87. Found: C 82.52, H 9.90. ^{1}H NMR (400 MHz, $CDCl_3$): δ = 0.81–0.95 (m, 6H, $-CH_3$), 1.18–1.46 (m, 18H, Ar–O–CH(CH_3)$(CH_2)_6CH_3$, –C≡C–$(CH_2)_2(CH_2)_3CH_3$), 1.48–1.80 (m, 5H, Ar–O–CH$(CH_3)(CH_2)_6CH_3$, –C≡C–$CH_2CH_2(CH_2)_3CH_3$), 2.38 (t, 2H, J = 7.2 Hz, –C≡C–$CH_2(CH_2)_4CH_3$), 4.21–4.39 (m, 1H, Ar–O–$CH(CH_3)(CH_2)_6CH_3$), 6.65–6.78 (m, 2H, Ar–H *meta* to C_6H_{13}–C≡C–), 7.28–7.53 (m, 2H, Ar–H *ortho* to C_6H_{13}–C≡C–). ^{13}C NMR (400 MHz, $CDCl_3$): δ = 14.1, 19.6, 22.5, 22.6, 25.5, 28.6, 29.2, 29.5, 29.8, 31.4, 31.8, 36.3, 74.1, 82.1, 88.5, 115.5, 118.1, 132.7, 158.0. HRMS (DART) calcd for $C_{23}H_{36}O$ [M + H$^+$]: 329.2839. Found: 329.2828. $[\alpha]^{25}_D$ −2.95° (*c* 1.0, $CHCl_3$).

(S)-Monomer 1 ((S)-M1). (***S***)-**M1** was synthesized in a similar way as (***rac***)-**M1**. Into a 100 mL three-necked flask were added compound **1** (1.05 g, 5.19 mmol) and TPP (1.25 g, 4.76 mmol) under argon gas and dissolved in THF (30 mL). In the addition funnel, a mixture of DEAD (2.41 g, 40 wt% in toluene, 4.75 mmol), (*R*)-(−)-2-nonanol (0.62 g, 4.32 mmol), and 30 mL THF was prepared. The reagents were then stirred overnight at room temperature. The reaction yielded a light yellow oil with a yield of 82% (1.17 g, 3.55 mmol).

Anal. Calcd for $(C_{23}H_{36}O)_n$ (328.53)$_n$: C, 84.09; H, 11.04; O, 4.87. Found: C 82.91, H 9.97. ^{1}H NMR (400 MHz, $CDCl_3$): δ = 0.80–1.00 (m, 6H, $-CH_3$), 1.20–1.51 (m, 18H, Ar–O–CH(CH_3)$(CH_2)_6CH_3$, –C≡C–$(CH_2)_2(CH_2)_3CH_3$), 1.52–1.79 (m, 5H, Ar–O–CH$(CH_3)(CH_2)_6CH_3$, –C≡C–$CH_2CH_2(CH_2)_3CH_3$), 2.38 (t, 2H, J = 6.8 Hz, –C≡C–$CH_2(CH_2)_4CH_3$), 4.27–4.34 (m, 1H, Ar–O–$CH(CH_3)(CH_2)_6CH_3$), 6.66–6.79 (m, 2H, Ar–H *meta* to C_6H_{13}–C≡C–), 7.26–7.52 (m, 2H, Ar–H *ortho* to C_6H_{13}–C≡C–). ^{13}C NMR (400 MHz, $CDCl_3$): δ = 14.1, 19.7, 22.5, 22.6, 25.5, 28.6, 29.2, 29.5, 29.5, 31.4, 31.8, 36.3, 73.9, 82.1, 88.5, 115.5, 118.1, 132.7, 157.5. HRMS (DART) calcd for $C_{23}H_{36}O$ [M + H$^+$]: 329.2839. Found: 329.2824. $[\alpha]^{25}_D$ +3.00° (*c* 1.0, $CHCl_3$).

(rac)-Monomer 2 ((rac)-M2). (***rac***)-**M2** was synthesized as follows. Into a 100 mL three-necked flask were added compound **2** (330 mg, 1.70 mmol) and TPP (491 mg, 1.87 mmol) under argon gas and dissolved in THF (30 mL). In the addition funnel, a mixture of DEAD (816 mg, 40 wt% in toluene, 1.87 mmol), 2-nonanol (246 mg, 1.70 mmol), and 20 mL THF were prepared. After dissolving the reagents under constant stirring, the flask was placed in an ice bath and the THF solution in the addition funnel was added dropwise to the solution in the flask. The solution was left overnight at room temperature. TLC indicated completion of the reaction. After evaporation of the solvent, the residue was washed with water and extracted with $CHCl_3$ (3×). The residue was dried over anhydrous Na_2SO_4, and the crude product was then purified by open column chromatography using $CHCl_3$ as eluent. The product was recrystallized from ethanol and dried under vacuum to give 0.37 g (1.14 mmol) of (***rac***)-**M2** as a white crystal. Yield = 67%.

Anal. Calcd for $(C_{23}H_{28}O)_n$ (320.47)$_n$: C, 86.20; H, 8.81; O, 4.99. Found: C 86.15, H 8.85. ^{1}H NMR (400 MHz, $CDCl_3$): δ = 0.88 (t, 3H, J = 6.8 Hz, $-CH_3$), 1.19–1.50 (m, 13H, Ar–O–CH(CH_3) $CH_2(CH_2)_5CH_3$), 1.52–1.68 (m, 2H, Ar–O–CH(CH_3) $CH_2(CH_2)_5CH_3$), 4.29–4.46 (m, 1H, Ar–O–$CH(CH_3)$-$CH_2(CH_2)_5CH_3$), 6.84 (d, 2H, J = 8.8 Hz, Ar–H *ortho* to –O–CH(CH_3)$(CH_2)_6CH_3$), 7.40–7.47 (m, 3H, Ar–H *meta* and *para* to –O–CH(CH_3)$(CH_2)_6CH_3$), 7.49–7.55 (m, 4H, Ar–H *ortho* to –C≡C–). ^{13}C NMR (400 MHz, $CDCl_3$): δ = 14.1, 19.7, 22.6, 25.5, 29.2, 29.5, 31.8, 36.4, 73.9, 87.8, 89.4, 114.8, 115.6, 127.7, 128.1, 131.3, 132.9, 158.2. HRMS (APCI) calcd for $C_{23}H_{28}O$ [M + H$^+$]: 321.2213. Found: 321.2211.

(R)-Monomer 2 ((R)-M2). (***R***)-**M2** was synthesized in a similar way as (***rac***)-**M2**. Into a 200 mL three-necked flask were added compound **2** (1.61 g, 8.29 mmol) and TPP (2.39 g, 9.12 mmol) under argon gas and dissolved in THF (60 mL). In the addition funnel, a mixture of DEAD (3.97 g, 40 wt% in toluene, 9.12 mmol), (*S*)-(+)-2-nonanol (1.20 g, 8.29 mmol), and 20 mL THF was prepared. The reagents were then stirred overnight at room temperature. The reaction yielded a white crystal with a yield of 82% (2.17 g, 6.80 mmol).

Anal. Calcd for $(C_{23}H_{28}O)_n$ (320.47)$_n$: C, 86.20; H, 8.81; O, 4.99. Found: C 86.26, H 8.83. ^{1}H NMR (400 MHz, $CDCl_3$): δ = 0.89 (t, 3H, J = 7.0 Hz, $-CH_3$), 1.29–1.53 (m, 13H, Ar–O–CH(CH_3) $CH_2(CH_2)_5CH_3$), 1.54–1.59 (m, 2H, Ar–O–CH(CH_3) $CH_2(CH_2)_5CH_3$), 4.35–4.37 (m, 1H, Ar–O–$CH(CH_3)$-$CH_2(CH_2)_5CH_3$), 6.86 (d, 2H, J = 8.6 Hz, Ar–H *ortho* to –O–CH(CH_3)$(CH_2)_6CH_3$), 7.24–7.34 (m, 3H, Ar–H *meta* and *para* to –O–CH(CH_3)$(CH_2)_6CH_3$), 7.43–7.50 (m, 4H, Ar–H *ortho* to –C≡C–). ^{13}C NMR (400 MHz, $CDCl_3$): δ = 14.1, 19.6, 22.6, 25.5, 29.5, 31.8, 36.4, 73.9, 87.7, 89.6, 115.0, 115.6, 123.7, 127.7, 128.1, 131.3, 132.9, 158.2. HRMS (APCI) calcd for $C_{23}H_{28}O$ [M + H$^+$]: 321.2213. Found: 321.2213. $[\alpha]^{25}_D$ +4.73° (*c* 1.0, $CHCl_3$).

(S)-Monomer 2 ((S)-M2). (***S***)-**M2** was synthesized in a similar way as (***rac***)-**M2**. Into a 200 mL three-necked flask were added compound **2** (0.65 g, 3.35 mmol) and TPP (0.97 g, 3.68 mmol) under argon gas and dissolved in THF (30 mL). In the addition funnel, a mixture of DEAD (1.88 g, 40 wt% in toluene, 3.68 mmol), (*R*)-(−)-2-nonanol (0.58 g, 4.02 mmol), and 20 mL THF was prepared. The reagents were then stirred overnight at room temperature. The reaction yielded a white crystal with a yield of 72% (0.77 g, 2.41 mmol).

Anal. Calcd for $(C_{23}H_{28}O)_n$ (320.47)$_n$: C, 86.20; H, 8.81; O, 4.99. Found: C 86.28, H 8.81. ^{1}H NMR (400 MHz, $CDCl_3$): δ = 0.88 (t, 3H, J = 7.2 Hz, $-CH_3$), 1.29–1.51 (m, 13H, Ar–O–CH(CH_3) $CH_2(CH_2)_5CH_3$), 1.53–1.57 (m, 2H, Ar–O–CH(CH_3) $CH_2(CH_2)_5CH_3$), 4.35–4.38 (m, 1H, Ar–O–$CH(CH_3)$-$CH_2(CH_2)_5CH_3$), 6.84 (d, 2H, J = 8.8 Hz, Ar–H *ortho* to –O–CH(CH_3)$(CH_2)_6CH_3$), 7.26–7.35 (m, 3H, Ar–H *meta* and *para* to –O–CH(CH_3)$(CH_2)_6CH_3$), 7.43–7.52 (m, 4H, Ar–H *ortho* to –C≡C–). ^{13}C NMR (400 MHz, $CDCl_3$): δ = 14.1, 19.7, 22.6, 25.5, 29.2, 31.8, 36.4, 73.9, 89.4, 91.6, 114.8, 115.6, 123.5, 127.7, 128.1, 131.3, 132.9, 156.9. HRMS (APCI) calcd for $C_{23}H_{28}O$ [M + H$^+$]: 321.2213. Found: 321.2213. $[\alpha]^{25}_D$ −4.95° (*c* 1.0, $CHCl_3$).

(rac)-Monomer 3 ((rac)-M3). (***rac***)-**M3** was synthesized as follows. Into a 100 mL three-necked flask were added compound **12** (1.10 g, 3.27 mmol) and TPP (0.94 g, 3.60 mmol) under argon gas and dissolved in THF (30 mL). In the addition funnel, a mixture of DEAD (1.82 g, 40 wt% in toluene, 3.60 mmol), 2-nonanol (0.61 g, 4.25 mmol), and 30 mL THF were prepared. After dissolving the reagents under constant stirring, the flask was placed in an ice bath and the THF solution in the addition funnel was added dropwise to the solution in the flask. The solution was left overnight at room temperature. TLC indicated completion of the reaction. After evaporation of the solvent, the residue was washed with water and extracted with $CHCl_3$ (3×). The residue was dried over anhydrous Na_2SO_4 and the crude product was then purified by open column chromatography using $CHCl_3$ as eluent. The product was evaporated and dried under vacuum to give compound (***rac***)-**M3** (0.95 g, 2.06 mmol) as a yellow oil. Yield = 63%.

dx.doi.org/10.1021/ja3086565 | *J. Am. Chem. Soc.* 2012, 134, 19795–19807

Anal. Calcd for $(C_{32}H_{46}O_2)_n$ (462.71)$_n$: C, 83.06; H, 10.02; O, 6.92. Found: C 82.30, H 10.38. ^{1}H NMR (400 MHz, $CDCl_3$): δ = 0.83−0.94 (m, 6H, $-CH_3$), 1.22−1.48 (m, 26H, Ar−O−CH(CH_3) $CH_2(CH_2)_5CH_3$), 1.51−1.79 (m, 4H, Ar−O−CH(CH_3) $CH_2(CH_2)_5CH_3$), 4.32−4.41 (m, 2H, Ar−O−$CH(CH_3)$-$CH_2(CH_2)_5CH_3$), 6.79−6.87 (d, 4H, J = 8.8 Hz, Ar−H *ortho* to −O−CH$(CH_3)(CH_2)_6CH_3$), 7.37−7.45 (d, 4H, J = 8.4 Hz, Ar−H *meta* to −O−CH$(CH_3)(CH_2)_6CH_3$). ^{13}C NMR (400 MHz, $CDCl_3$): δ = 14.1, 19.6, 22.6, 25.5, 29.2, 29.5, 31.8, 36.4, 73.8, 87.8, 115.3, 115.6, 132.7, 157.9. HRMS (APCI) calcd for $C_{32}H_{46}O_2$ [M + H$^+$]: 463.3571. Found: 463.3570.

(R)-Monomer 3 ((R)-M3). (***R***)**-M3** was synthesized in a similar way as (***rac***)**-M3**. Into a 100 mL three-necked flask were added compound **13** (1.30 g, 3.86 mmol) and TPP (1.11 g, 4.25 mmol) under argon gas and dissolved in THF (30 mL). In the addition funnel, a mixture of DEAD (2.15 g, 40 wt% in toluene, 4.25 mmol), (*S*)-(+)-2-nonanol (0.72 g, 5.02 mmol), and 30 mL THF was prepared. The reagents were then stirred overnight at room temperature. The product was evaporated and dried under vacuum to give compound (***R***)**-M3** (1.25 g, 2.69 mmol) as a yellow oil. Yield = 70%.

Anal. Calcd for $(C_{32}H_{46}O_2)_n$ (462.71)$_n$: C, 83.06; H, 10.02; O, 6.92. Found: C 81.83, H 9.78. ^{1}H NMR (400 MHz, $CDCl_3$): δ = 0.81−0.92 (m, 6H, $-CH_3$), 1.19−1.48 (m, 26H, Ar−O−CH(CH_3) $CH_2(CH_2)_5CH_3$), 1.50−1.79 (m, 4H, Ar−O−CH(CH_3) $CH_2(CH_2)_5CH_3$), 4.31−4.41 (m, 2H, Ar−O−$CH(CH_3)$-$CH_2(CH_2)_5CH_3$), 6.79−6.87 (d, 4H, J = 8.8 Hz, Ar−H *ortho* to −O−CH$(CH_3)(CH_2)_6CH_3$), 7.38−7.46 (d, 4H, J = 8.0 Hz, Ar−H *meta* to −O−CH$(CH_3)(CH_2)_6CH_3$). ^{13}C NMR (400 MHz, $CDCl_3$): δ = 14.1, 19.7, 22.6, 25.5, 29.2, 29.5, 31.8, 36.4, 73.9, 87.8, 115.3, 115.6, 132.7, 157.9. HRMS (APCI) calcd for $C_{32}H_{46}O_2$ [M + H$^+$]: 463.3571. Found: 463.3571. $[\alpha]^{25}_D$ +7.87° (*c* 1.0, $CHCl_3$).

(S)-Monomer 3 ((S)-M3). (***S***)**-M3** was synthesized in a similar way as (***rac***)**-M3**. Into a 100 mL three-necked flask were added compound **14** (488 mg, 1.33 mmol) and TPP (384 g, 1.46 mmol) under argon gas and dissolved in THF (20 mL). In the addition funnel, a mixture of DEAD (637 mg, 40 wt% in toluene, 1.46 mmol), (*R*)-(−)-2-nonanol (192 mg, 1.33 mmol), and 20 mL THF was prepared. The reagents were then stirred overnight at room temperature. The product was evaporated and dried under vacuum to give compound (***S***)**-M3** (0.38 g, 0.81 mmol) as a yellow oil. Yield = 61%.

Anal. Calcd for $(C_{32}H_{46}O_2)_n$ (462.71)$_n$: C, 83.06; H, 10.02; O, 6.92. Found: C 82.16, H 10.52. ^{1}H NMR (400 MHz, $CDCl_3$): δ = 0.81−0.96 (m, 6H, $-CH_3$), 1.19−1.50 (m, 26H, Ar−O−CH(CH_3) $CH_2(CH_2)_5CH_3$), 1.52−1.79 (m, 4H, Ar−O−CH(CH_3) $CH_2(CH_2)_5CH_3$), 4.25−4.45 (m, 2H, Ar−O−$CH(CH_3)$-$CH_2(CH_2)_5CH_3$), 6.77−6.96 (d, 4H, J = 8.8 Hz, Ar−H *ortho* to −O−CH$(CH_3)(CH_2)_6CH_3$), 7.36−7.48 (d, 4H, J = 8.8 Hz, Ar−H *meta* to −O−CH$(CH_3)(CH_2)_6CH_3$). ^{13}C NMR (400 MHz, $CDCl_3$): δ = 14.1, 19.7, 22.6, 25.5, 29.2, 29.6, 31.8, 36.4, 73.9, 87.8, 115.3, 115.6, 132.7, 157.9. HRMS (APCI) calcd for $C_{32}H_{46}O_2$ [M + H$^+$]: 463.3571. Found: 463.3571. $[\alpha]^{25}_D$ −7.26° (*c* 1.0, $CHCl_3$).

(rac)-PA1. (***rac***)**-PA1** was synthesized as follows. Toluene (1.0 mL), WCl_6 (17.1 mg, 0.04 mmol), and *n*-Ph_4Sn (36.8 mg, 0.08 mmol) were added under argon into a Schlenk flask. The catalyst mixture was stirred at 80 °C for 30 min, and then (***rac***)**-M1** (0.28 g, 0.86 mmol) was dissolved in 1 mL toluene and was then added to the reaction mixture. The reaction mixture was stirred at 80 °C for 24 h. The mixture was cooled to room temperature and was added dropwise to 800 mL of methanol under stirring. The polymer precipitate was stirred for 24 h, which was then filtered and dried in vacuo. A yellowish solid was obtained with a yield of 8.6% (23.3 mg, 0.08 mmol). M_w = 48 300; M_w/M_n = 2.1 (GPC, PS calibration).

Anal. Calcd for $(C_{23}H_{28}O)_n$ (328.53)$_n$: C, 84.09; H, 11.04; O, 4.87. Found: C 81.23, H 10.34. ^{1}H NMR (400 MHz, $CDCl_3$): δ = 0.50−0.95 (br, 6H, $-CH_3$), 0.97−1.84 (br, 25H, Ar−O−CH(CH_3) $(CH_2)_6CH_3$, −C≡C−$(CH_2)_2(CH_2)_3CH_3$, Ar−O−CH(CH_3) $(CH_2)_6CH_3$, −C≡C−$CH_2CH_2(CH_2)_3CH_3$, −C≡C−$CH_2(CH_2)_4CH_3$), 3.81−4.49 (br, 1H, Ar−O−$CH(CH_3)(CH_2)_6CH_3$), 7.21−7.39 (br, 4H, Ar−H). ^{13}C NMR (400 MHz, $CDCl_3$): δ = 14.0, 19.1, 21.5, 22.6, 23.9, 29.3, 30.7, 31.8, 73.0, 80.0, 100.5, 114.0, 133.2, 155.1.

(R)-PA1. (***R***)**-PA1** was synthesized in a similar way as (***rac***)**-PA1**. Polymerization of (***R***)**-M1** (0.35 g, 1.06 mmol) yielded a yellowish solid with a yield of 41% (0.15 g, 0.44 mmol). M_w = 26 700; M_w/M_n = 1.7 (GPC, PS calibration).

Anal. Calcd for $(C_{23}H_{28}O)_n$ (328.53)$_n$: C, 84.09; H, 11.04; O, 4.87. Found: C, 83.33; H, 11.65. ^{1}H NMR (400 MHz, $CDCl_3$): δ = 0.55−0.98 (br, 6H, $-CH_3$), 1.00−1.81 (br, 25H, Ar−O−CH(CH_3) $(CH_2)_6CH_3$, −C≡C−$(CH_2)_2(CH_2)_3CH_3$, Ar−O−CH(CH_3) $(CH_2)_6CH_3$, −C≡C−$CH_2CH_2(CH_2)_3CH_3$, −C≡C−$CH_2(CH_2)_4CH_3$), 3.80−4.47 (br, 1H, Ar−O−$CH(CH_3)(CH_2)_6CH_3$), 7.19−7.31 (br, 4H, Ar−H). ^{13}C NMR (400 MHz, $CDCl_3$): δ = 14.0, 19.6, 22.1, 22.6, 23.1, 29.3, 29.7, 32.0, 71.2, 80.7, 102.7, 114.1, 134.5, 157.3. $[\alpha]^{25}_D$ −241° (*c* 1.0, $CHCl_3$).

(S)-PA1. (***S***)**-PA1** was synthesized in a similar way as (***rac***)**-PA1**. Polymerization of (***S***)**-M1** (0.35 g, 1.06 mmol) yielded a yellowish solid with a yield of 5.9% (20.8 mg, 0.06 mmol). M_w = 44 400; M_w/M_n = 1.7 (GPC, PS calibration).

Anal. Calcd for $(C_{23}H_{28}O)_n$ (328.53)$_n$: C, 84.09; H, 11.04; O, 4.87. Found: C 79.09, H 11.24. ^{1}H NMR (400 MHz, $CDCl_3$): δ = 0.55−0.99 (br, 6H, $-CH_3$), 1.10−1.85 (br, 25H, Ar−O−CH(CH_3) $(CH_2)_6CH_3$, −C≡C−$(CH_2)_2(CH_2)_3CH_3$, Ar−O−CH(CH_3) $(CH_2)_6CH_3$, −C≡C−$CH_2CH_2(CH_2)_3CH_3$, −C≡C−$CH_2(CH_2)_4CH_3$), 3.79−4.51 (br, 1H, Ar−O−$CH(CH_3)(CH_2)_6CH_3$), 7.15−7.32 (br, 4H, Ar−H). ^{13}C NMR (400 MHz, $CDCl_3$): δ = 14.1, 18.5, 22.3, 22.5, 23.2, 29.1, 30.2, 31.8, 73.6, 82.4, 101.3, 113.7, 130.7, 157.7. $[\alpha]^{25}_D$ +247° (*c* 1.0, $CHCl_3$).

(rac)-PA2. (***rac***)**-PA2** was synthesized in a similar way as (***rac***)**-PA1**. Polymerization of (***rac***)**-M2** (0.28 g, 0.86 mmol) yielded a greenish powder with a yield of 45% (0.12 g, 0.39 mmol). M_w = 22 000; M_w/M_n = 2.4 (GPC, PS calibration).

Anal. Calcd for $(C_{23}H_{28}O)_n$ (320.47)$_n$: C, 86.20; H, 8.81; O, 4.99. Found: C 83.96, H 8.65. ^{1}H NMR (400 MHz, $CDCl_3$): δ = 0.81−0.95 (br, 3H, $-CH_3$), 1.20−1.61 (br, 15H, Ar−O−CH(CH_3) $CH_2(CH_2)_5CH_3$, and Ar−O−CH$(CH_3)CH_2(CH_2)_5CH_3$), 3.96−4.21 (br, 1H, Ar−O−$CH(CH_3)CH_2(CH_2)_5CH_3$), 6.91−7.61 (br, 9H, Ar−H). ^{13}C NMR (400 MHz, $CDCl_3$): δ = 14.1, 19.5, 23.5, 25.4, 31.0, 33.7, 85.5, 114.9, 122.5, 124.7, 131.5, 151.6.

(R)-PA2. (***R***)**-PA2** was synthesized synthesized in a similar way as (***rac***)**-PA1**. Polymerization of (***R***)**-M2** (0.30 g, 0.9 mmol) yielded a greenish powder with a yield of 6% (16.7 mg, 0.06 mmol). M_w = 23 000; M_w/M_n = 2.1 (GPC, PS calibration).

Anal. Calcd for $(C_{23}H_{28}O)_n$ (320.47)$_n$: C, 86.20; H, 8.81; O, 4.99. Found: C 81.56, H 9.57. ^{1}H NMR (400 MHz, $CDCl_3$): δ = 0.80−1.00 (br, 3H, $-CH_3$), 1.05−1.80 (br, 15H, Ar−O−CH(CH_3) $CH_2(CH_2)_5CH_3$, and Ar−O−CH$(CH_3)CH_2(CH_2)_5CH_3$), 3.95−4.18 (br, 1H, Ar−O−$CH(CH_3)CH_2(CH_2)_5CH_3$), 6.92−7.52 (br, 9H, Ar−H). ^{13}C NMR (400 MHz, $CDCl_3$): δ = 14.1, 19.6, 22.7, 25.4, 29.5, 32.0, 85.1, 114.9, 122.6, 124.7, 139.8, 156.6. $[\alpha]^{25}_D$ +229° (*c* 1.0, $CHCl_3$).

(S)-PA2. (***S***)**-PA2** was synthesized in a similar way as (***rac***)**-PA1**. Polymerization of (***S***)**-M2** (0.30 g, 0.94 mmol) yielded a greenish powder with a yield of 80% (0.24 g, 0.75 mmol). M_w = 25 000 M_w/M_n = 2.3 (GPC, PS calibration).

Anal. Calcd for $(C_{23}H_{28}O)_n$ (320.47)$_n$: C, 86.20; H, 8.81; O, 4.99. Found: C 83.00, H 8.87. ^{1}H NMR (400 MHz, $CDCl_3$): δ = 0.82−0.98 (br, 3H, $-CH_3$), 1.03−1.78 (br, 15H, Ar−O−CH(CH_3) $CH_2(CH_2)_5CH_3$, and Ar−O−CH$(CH_3)CH_2(CH_2)_5CH_3$), 3.90−4.15 (br, 1H, Ar−O−$CH(CH_3)CH_2(CH_2)_5CH_3$), 6.95−7.50 (br, 9H, Ar−H). ^{13}C NMR (400 MHz, $CDCl_3$): δ = 14.1, 19.6, 22.7, 25.4, 29.5, 83.1, 114.2, 122.0, 139.8, 152.8. $[\alpha]^{25}_D$ −226° (*c* 1.0, $CHCl_3$).

(rac)-PA3. (***rac***)**-PA3** was synthesized in a similar way as (***rac***)**-PA1**. Polymerization of (***rac***)**-M3** (0.30 g, 0.65 mmol) yielded a greenish powder with a yield of 7% (21.7 mg, 0.05 mmol). M_w = 13 400; M_w/M_n = 2.0 (GPC, PS calibration).

Anal. Calcd for $(C_{32}H_{46}O_2)_n$ (462.71)$_n$: C, 83.06; H, 10.02; O, 6.92. Found: C 79.40, H 8.91. ^{1}H NMR (400 MHz, $CDCl_3$): δ = 0.72−0.96 (br, 6H, $-CH_3$), 0.98−1.80 (br, 30H, Ar−O−CH(CH_3) $CH_2(CH_2)_5CH_3$, Ar−O−CH$(CH_3)CH_2(CH_2)_5CH_3$), 3.95−4.20 (br,

2H, Ar−O−*CH*(CH$_3$)CH$_2$(CH$_2$)$_5$CH$_3$), 5.90−6.20 (br, 4H, Ar−H *ortho* to −O−CH(CH$_3$)CH$_2$(CH$_2$)$_5$CH$_3$), 7.08−7.40 (br, 4H, Ar−H *meta* to −O−CH(CH$_3$)CH$_2$(CH$_2$)$_5$CH$_3$). ^{13}C NMR (400 MHz, CDCl$_3$): δ = 14.1, 20.4, 22.5, 27.3, 30.0, 32.2, 36.1, 74.3, 87.4, 123.4, 132.3, 157.8.

(R)-PA3. (***R***)-**PA3** was synthesized in a similar way as (***rac***)-**PA1**. Polymerization of (***R***)-**M3** (0.30 g, 0.65 mmol) yielded a greenish powder with a yield of 11% (32.6 mg, 0.07 mmol). M_w = 12 700; M_w/M_n = 2.8 (GPC, PS calibration).

Anal. Calcd for $(C_{32}H_{46}O_2)_n$ $(462.71)_n$: C, 83.06; H, 10.02; O, 6.92. Found: C 78.17, H 9.58. ^{1}H NMR (400 MHz, CDCl$_3$): δ = 0.79−0.98 (br, 6H, −*CH*$_3$), 0.99−1.71 (br, 30H, Ar−O−CH(*CH*$_3$)CH$_2$(*CH*$_2$)$_5$CH$_3$, Ar−O−CH(CH$_3$)*CH*$_2$(CH$_2$)$_5$CH$_3$), 4.00−4.20 (br, 2H, Ar−O−*CH*(CH$_3$)CH$_2$(CH$_2$)$_5$CH$_3$), 5.91−6.22 (br, 4H, Ar−H *ortho* to −O−CH(CH$_3$)CH$_2$(CH$_2$)$_5$CH$_3$), 7.18−7.40 (br, 4H, Ar−H *meta* to −O−CH(CH$_3$)CH$_2$(CH$_2$)$_5$CH$_3$). ^{13}C NMR (400 MHz, CDCl$_3$): δ = 14.1, 20.7, 22.7, 27.4, 29.9, 31.1, 36.2, 74.9, 85.4, 122.4, 131.4, 158.1. $[\alpha]^{25}_D$ +2080° (*c* 1.0, CHCl$_3$).

(S)-PA3. (***S***)-**PA3** was synthesized in a similar way as (***rac***)-**PA1**. Polymerization of (***S***)-**M3** (0.30 g, 0.65 mmol) yielded a greenish powder with a yield of 30% (90.1 mg, 0.19 mmol). M_w = 14 000; M_w/M_n = 2.3 (GPC, PS calibration).

Anal. Calcd for $(C_{32}H_{46}O_2)_n$ $(462.71)_n$: C, 83.06; H, 10.02; O, 6.92. Found: C 82.91, H 10.58. ^{1}H NMR (400 MHz, CDCl$_3$): δ = 0.75−0.98 (br, 6H, −*CH*$_3$), 1.00−1.69 (br, 30H, Ar−O−CH(*CH*$_3$)CH$_2$(*CH*$_2$)$_5$CH$_3$, Ar−O−CH(CH$_3$)*CH*$_2$(CH$_2$)$_5$CH$_3$), 3.96−4.19 (br, 2H, Ar−O−*CH*(CH$_3$)CH$_2$(CH$_2$)$_5$CH$_3$), 5.94−6.22 (br, 4H, Ar−H *ortho* to −O−CH(CH$_3$)CH$_2$(CH$_2$)$_5$CH$_3$), 7.19−7.38 (br, 4H, Ar−H *meta* to −O−CH(CH$_3$)CH$_2$(CH$_2$)$_5$CH$_3$). ^{13}C NMR (400 MHz, CDCl$_3$): δ = 14.1, 21.4, 22.7, 27.7, 29.3, 32.0, 36.5, 74.1, 82.2, 119.4, 131.4, 157.9. $[\alpha]^{25}_D$ −2158° (*c* 1.0, CHCl$_3$).

■ ASSOCIATED CONTENT

Supporting Information

Synthetic routes of the precursor compounds, representative results of X-ray diffraction (XRD), polarizing optical microscope (POM), and chiroptical properties (CD and CPL). This material is available free of charge via the Internet at http://pubs.acs.org.

■ AUTHOR INFORMATION

Corresponding Author

akagi@fps.polym.kyoto-u.ac.jp

Notes

The authors declare no competing financial interest.

■ ACKNOWLEDGMENTS

The authors thank Prof. Kenji Saijo (Kyoto University) for the XRD measurements of the polymers. This work was supported by a Grant-in-Aid for Science Research (S) (No. 20225007) from the Ministry of Education, Culture, Sports, Science and Technology, Japan.

■ REFERENCES

(1) (a) Grell, M.; Bradley, D. D. C. *Adv. Mater.* **1999**, *11*, 895−905. (b) Schadt, M. *Annu. Rev. Mater. Sci.* **1997**, *27*, 305−379. (c) Emeis, C. A.; Oosterhoff, L. J. *Chem. Phys. Lett.* **1967**, *1*, 129−132. (d) Dyreklev, P.; Berggren, M.; Inganäs, O.; Andersson, M. R.; Wennerström, O.; Hjertberg, T. *Adv. Mater.* **1995**, *7*, 43−45. (e) Liu, J.; Su, H.; Meng, L.; Zhao, Y.; Deng, C.; Ng, J. C. Y.; Lu, P.; Faisal, M.; Lam, J. W. Y.; Huang, X.; Wu, H.; Wong, K. S.; Tang, B. Z. *Chem. Sci.* **2012**, *3*, 2737−2747.

(2) Peeters, E.; Christiaans, M. P. T.; Janssen, R. A. J.; Schoo, H. F. M.; Dekkers, H. P. J. M.; Meijer, E. W. *J. Am. Chem. Soc.* **1997**, *119*, 9909−9910.

(3) Langeveld-Voss, B. M. W.; Janssen, R. A. J.; Christiaans, M. P. T.; Meskers, S. C. J.; Dekkers, H. P. J. M.; Meijer, E. W. *J. Am. Chem. Soc.* **1996**, *118*, 4908−4909.

(4) Oda, M.; Nothofer, H. G.; Lieser; Scherf, U.; Meskers, S. C. J.; Neher, D. *Adv. Mater.* **2000**, *12*, 362−365.

(5) (a) Chen, S. H.; Conger, B. M.; Mastrangelo, J. C.; Kende, A. S.; Kim, D. U. *Macromolecules* **1998**, *31*, 8051−8057. (b) Wilson, J.; Steffen, W.; McKenzie, T. G.; Lieser, G.; Oda, M.; Neher, D.; Bunz, U. H. F. *J. Am. Chem. Soc.* **2002**, *124*, 6830−6831. (c) Oda, M.; Nothofer, H. G.; Scherf, U.; Sunjic, V.; Richter, D.; Regenstein, W.; Neher, D. *Macromolecules* **2002**, *35*, 6792−6798. (d) Satrijo, A.; Meskers, S. C. J.; Swager, T. M. *J. Am. Chem. Soc.* **2006**, *128*, 9030−9031. (e) Watanabe, K.; Osaka, I.; Yorozuya, S.; Akagi, K. *Chem. Mater.* **2012**, *24*, 1011−1024. (f) Watanabe, K.; Iida, H.; Akagi, K. *Adv. Mater.* **2012**, DOI: 10.1002/adma.201203155.

(6) (a) Goto, H. *Macromolecules* **2007**, *40*, 1377−1385. (b) Haraguchi, S.; Numata, M.; Li, C.; Nakano, Y.; Fujiki, M.; Shinkai, S. *Chem. Lett.* **2009**, *38*, 254−255.

(7) Thermotropic LCs exhibit phase transitions as a function of temperature, while lyotropic LCs exhibit phase transitions as a function of concentration of the LC molecules in a solvent. The nematic LC (N-LC) has a mesophase where the LC molecules have no positional ordering but align along one direction. The N*-LC has an orientation ordering similar to the N-LC, but the director of each domain rotates along a helical axis resulting in a right-handed (clockwise) or left-handed (counter-clockwise) screw structure.

(8) Bobrovsky, A. Y.; Boiko, N. I.; Shibaev, V. P.; Wendorff, J. H. *Adv. Mater.* **2003**, *15*, 282−287.

(9) Pollmann, P.; Mainusch, K. J.; Stegemeyer, H. *Z. Phys. Chem. (Leipzig)* **1976**, *103*, 295−309.

(10) (a) Chen, S. H.; Katsis, D.; Schmid, A. W.; Mastrangelo, J. C.; Tsutsui, T.; Blanton, T. N. *Nature* **1999**, *397*, 506−508. (b) Grell, M.; Oda, M.; Whitehead, K. S.; Asimakis, A.; Neher, D.; Bradley, D. D. C. *Adv. Mater.* **2001**, *13*, 577−580.

(11) Il'chishin, I. P.; Tikhonov, E. A.; Tishchenko, V. G.; Shpak, M. T. *JETP Lett.* **1981**, *32*, 24−27.

(12) Furumi, S. *Chem. Rec.* **2010**, *10*, 394−408.

(13) (a) Akagi, K.; Piao, G.; Kaneko, S.; Sakamaki, K.; Shirakawa, H.; Kyotani, M. *Science* **1998**, *282*, 1683−1686. (b) Akagi, K.; Piao, G.; Kaneko, S.; Higuchi, I.; Shirakawa, H.; Kyotani, M. *Synth. Met.* **1999**, *102*, 1406−1409. (c) Akagi, K.; Guo, S.; Mori, T.; Goh, M.; Piao, G.; Kyotani, M. *J. Am. Chem. Soc.* **2005**, *127*, 14647−14654. (d) Akagi, K. *Polym. Int.* **2007**, *56*, 1192−1199.

(14) Iida, H.; Nakamura, A.; Inoue, Y.; Akagi, K. *Synth. Met.* **2003**, *135*, 91−92.

(15) (a) Green, M. M.; Park, J. W.; Sato, T.; Teramoto, A.; Lifson, S.; Selinger, R. L. B.; Selinger, J. V. *Angew. Chem., Int. Ed.* **1999**, *38*, 3138−3154. (b) Siekmeyer, M.; Steinmeier, H.; Zugenmaier, P. *Makromol. Chem.* **1989**, *190*, 1037−1045. (c) Robinson, C.; Ward, J. C. *Nature* **1957**, *180*, 1183−1184. (d) Tsujita, Y.; Yamanaka, I.; Takizawa, A. *Polymer J.* **1979**, *11*, 749−754. (e) Livolant, F.; Bouligand, Y. *J. Phys. (Paris)* **1986**, *47*, 1813−1827. (f) Bawden, F. C.; Pirie, N. W.; Bernal, J. D.; Fankuchen, I. *Nature* **1936**, *138*, 1051−1052. (g) Dogic, Z.; Fraden, S. *Phys. Rev. Lett.* **1997**, *78*, 2417−2420.

(16) (a) Lam, J. W. Y.; Tang, B. Z. *J. Polym. Sci., Part A: Polym. Chem.* **2003**, *41*, 2607−2629. (b) Liu, J.; Lam, J. W. Y.; Tang, B. Z. *Chem. Rev.* **2009**, *109*, 5799−5867.

(17) (a) Kwak, G.; Minakuchi, M.; Sakaguchi, T.; Masuda, T.; Fujiki, M. *Chem. Mater.* **2007**, *19*, 3654−3661. (b) Kwak, G.; Minakuchi, M.; Sakaguchi, T.; Masuda, T.; Fujiki, M. *Macromolecules* **2008**, *41*, 2743−2746. (c) Tsuchihara, K.; Fukushima, T. *Macromolecules* **2009**, *42*, 5453−5460. (d) Lee, D.; Kim, H.; Suzuki, N.; Fujiki, M.; Lee, C.-L.; Lee, W.-E.; Kwak, G. *Chem. Commun.* **2012**, *48*, 9275−9277.

(18) San Jose, B. A.; Matsushita, S.; Moroishi, Y.; Akagi, K. *Macromolecules* **2011**, *44*, 6288−6302.

(19) (a) Sonogashira, K.; Tohda, Y.; Hagihara, N. *Tetrahedron Lett.* **1975**, *16*, 4467−4470. (b) Sonogashira, K. *J. Organomet. Chem.* **2002**, *653*, 46−49. (c) Mitsunobu, O.; Yamada, M. *Bull. Chem. Soc. Jpn.*

1967, *40*, 2380−2382. (d) Williamson, A. W. *J. Chem. Soc.* **1852**, *4*, 229−239.

(20) *Textures of Liquid Crystals*; Dierking, I., Ed.; Wiley-VCH: Weinheim, 2003.

(21) The length of the **PA2** nonyloxy phenyl side chain was calculated using molecular mechanics calculations. The side chain with the nonyloxy phenyl moiety has a length (L_1) computed as 15 Å. The XRD peak distance of 15 Å observed in the (***S***)-**PA2** N*-LC film can be assigned as the average polymer interchain distance approximate to that of the side chain length, $d \approx L_1$, within the N*-LC domain. XRD analysis on the N-LC film of (***rac***)-**PA2** and N*-LC film of (***S***)-**D1**/(***rac***)-**PA2** showed similar XRD profiles (Figure S2), which suggest that the measured distances of 15−17 Å can be correlated to the polymer interchain distance−regardless of the LC phase. The observed XRD patterns are similar to the XRD profiles of other reports of PDPA showing lyotropic liquid crystallinity.[17a,b]

(22) It was observed that the N*-LC phase of (***S***)-**PA2** and (***S***)-**D1**/(***rac***)-**PA2**, have different helical half-pitches of 1.5 and 2.0 μm, respectively (Figures 1a and 2b). This shows that the N*-LC phase of (***S***)-**PA2** has a more twisted helical ordering on a microscopic level, given the same lyotropic LC concentration. This difference can be attributed to the type of the chiral dopant used. In the N*-LC phase of (***S***)-**PA2**, the chiral dopant is the chiral nonyloxy moiety with an asymmetric type chirality. On the other hand, for the N*-LC phase of (***S***)-**D1**/(***rac***)-**PA2** the chiral dopant (***S***)-**D1** has an axial type chirality. In the N*-LC phase of (***S***)-**D1**/(***rac***)-**PA2**, the chiral dopant is in between the nematic LC layers where it directs the layers into a helical arrangement.

(23) (a) Shukla, A.; Mazumdar, S. *Phy. Rev. Lett.* **1999**, *19*, 3944−3947. (b) Hidayat, R.; Fujii, A.; Ozaki, M.; Teraguchi, M.; Masuda, T.; Yoshino, K. *Synth. Met.* **2001**, *119*, 597−598. (c) Shukla, A.; Ghosh, H.; Mazumdar, S. *Synth. Met.* **2001**, *116*, 87−90. (d) Ghosh, H.; Shukla, A.; Mazumdar, S. *Phys. Rev. B.* **2000**, *19*, 12763−12774. (e) Vardeny, Z. V., Korovyanko, O. In *Handbook of Conducting Polymers, Conjugated Polymers*, 3rd ed.; Skotheim, T. A., Reynolds, J. R., Eds.; CRC Press: New York, 2007; pp 22-1−22-74.

(24) For the preparation of **D1**-doped (***rac***)-**PA2** and (***rac***)-**PA3** N*-LC films, the (***R***)-/(***S***)-**D1** chiral dopant at 10 wt%, was added to the polymers and then the solution was dissolved in toluene (5−10 wt%) to form a lyotropic LC state. The lyotropic LC solution was cast onto a quartz plate, which was then exposed under toluene vapor and allowed to dry slowly at room temperature.

(25) It is expected that in low concentration solutions of PDPA in toluene, the polymer main chains will lose the cooperative ordering of the LC phase and will behave like an isotropic liquid. To verify this we measured the UV−vis and CD spectra of (***rac***)-/(***R***)-/(***S***)-**PA2** in low concentration solution (1.2×10^{-4} M) in toluene. The spectra on Figure S4 reveals monosignate Cotton effects that reflect the intrachain helicity of **PA2**, similar to **PA2** in chloroform solution (Figure 4b).

(26) CD measurements in cast films and N*-LC films were taken on all the four possible orientations (horizontal and vertical) of the quartz plates and the results were compared. This procedure was performed to check for sample orientation dependence of the CD measurements. CD results of the samples showed no sample orientation dependence.

(27) (a) Harada, N.; Nakanishi, K.*Circular Dichroic Spectroscopy: Exciton Coupling in Organic Steroechemistry*; University Science Books: Sausalito, CA, 1983. (b) Berova, N.; Nakanishi, K. In *Circular Dichroism: Principles and Applications*, 2nd ed.; Berova, N., Nakanishi, K., Woody, R., Eds.; John Wiley and Sons, Inc.: New York, 2000; Chap. 12, pp 337−382.

(28) For all cast films and N*-LC films, the linear dichroism was much less than 0.01, which discounts that the large *g*-values are due to measurement artifacts. In addition, measurements were taken on all the four possible orientations (horizontal and vertical), and no orientation dependence was apparent.